CLEO CONF 02-09
ICHEP02 ABS931

Measurement of the $B \to \pi \ell \nu$ and $B \to \rho(\omega) \ell \nu$ Branching Fractions with Reduced Model Dependence and Extraction of $|V_{ub}|$*

N. E. Adam,[1] J. P. Alexander,[1] K. Berkelman,[1] V. Boisvert,[1] D. G. Cassel,[1] P. S. Drell,[1] J. E. Duboscq,[1] K. M. Ecklund,[1] R. Ehrlich,[1] L. Gibbons,[1] B. Gittelman,[1] S. W. Gray,[1] D. L. Hartill,[1] B. K. Heltsley,[1] L. Hsu,[1] C. D. Jones,[1] J. Kandaswamy,[1] D. L. Kreinick,[1] A. Magerkurth,[1] H. Mahlke-Krüger,[1] T. O. Meyer,[1] N. B. Mistry,[1] E. Nordberg,[1] J. R. Patterson,[1] D. Peterson,[1] J. Pivarski,[1] D. Riley,[1] A. J. Sadoff,[1] H. Schwarthoff,[1] M. R. Shepherd,[1] J. G. Thayer,[1] D. Urner,[1] G. Viehhauser,[1] A. Warburton,[1] M. Weinberger,[1] S. B. Athar,[2] P. Avery,[2] L. Breva-Newell,[2] V. Potlia,[2] H. Stoeck,[2] J. Yelton,[2] G. Brandenburg,[3] D. Y.-J. Kim,[3] R. Wilson,[3] K. Benslama,[4] B. I. Eisenstein,[4] J. Ernst,[4] G. D. Gollin,[4] R. M. Hans,[4] I. Karliner,[4] N. Lowrey,[4] C. Plager,[4] C. Sedlack,[4] M. Selen,[4] J. J. Thaler,[4] J. Williams,[4] K. W. Edwards,[5] R. Ammar,[6] D. Besson,[6] X. Zhao,[6] S. Anderson,[7] V. V. Frolov,[7] Y. Kubota,[7] S. J. Lee,[7] S. Z. Li,[7] R. Poling,[7] A. Smith,[7] C. J. Stepaniak,[7] J. Urheim,[7] Z. Metreveli,[8] K.K. Seth,[8] A. Tomaradze,[8] P. Zweber,[8] S. Ahmed,[9] M. S. Alam,[9] L. Jian,[9] M. Saleem,[9] F. Wappler,[9] E. Eckhart,[10] K. K. Gan,[10] C. Gwon,[10] T. Hart,[10] K. Honscheid,[10] D. Hufnagel,[10] H. Kagan,[10] R. Kass,[10] T. K. Pedlar,[10] J. B. Thayer,[10] E. von Toerne,[10] T. Wilksen,[10] M. M. Zoeller,[10] H. Muramatsu,[11] S. J. Richichi,[11] H. Severini,[11] P. Skubic,[11] S.A. Dytman,[12] J.A. Mueller,[12] S. Nam,[12] V. Savinov,[12] S. Chen,[13] J. W. Hinson,[13] J. Lee,[13] D. H. Miller,[13] V. Pavlunin,[13] E. I. Shibata,[13] I. P. J. Shipsey,[13] D. Cronin-Hennessy,[14] A.L. Lyon,[14] C. S. Park,[14] W. Park,[14] E. H. Thorndike,[14] T. E. Coan,[15] Y. S. Gao,[15] F. Liu,[15] Y. Maravin,[15] R. Stroynowski,[15] M. Artuso,[16] C. Boulahouache,[16] K. Bukin,[16] E. Dambasuren,[16] K. Khroustalev,[16] R. Mountain,[16] R. Nandakumar,[16] T. Skwarnicki,[16] S. Stone,[16] J.C. Wang,[16] A. H. Mahmood,[17] S. E. Csorna,[18] I. Danko,[18] G. Bonvicini,[19] D. Cinabro,[19] M. Dubrovin,[19] S. McGee,[19] A. Bornheim,[20] E. Lipeles,[20] S. P. Pappas,[20] A. Shapiro,[20] W. M. Sun,[20] A. J. Weinstein,[20] R. Mahapatra,[21] R. A. Briere,[22] G. P. Chen,[22] T. Ferguson,[22] G. Tatishvili,[22] and H. Vogel[22]

(CLEO Collaboration)

[1]Cornell University, Ithaca, New York 14853
[2]University of Florida, Gainesville, Florida 32611
[3]Harvard University, Cambridge, Massachusetts 02138
[4]University of Illinois, Urbana-Champaign, Illinois 61801
[5]Carleton University, Ottawa, Ontario, Canada K1S 5B6 and the Institute of Particle Physics, Canada M5S 1A7
[6]University of Kansas, Lawrence, Kansas 66045
[7]University of Minnesota, Minneapolis, Minnesota 55455
[8]Northwestern University, Evanston, Illinois 60208
[9]State University of New York at Albany, Albany, New York 12222
[10]Ohio State University, Columbus, Ohio 43210
[11]University of Oklahoma, Norman, Oklahoma 73019
[12]University of Pittsburgh, Pittsburgh, Pennsylvania 15260
[13]Purdue University, West Lafayette, Indiana 47907
[14]University of Rochester, Rochester, New York 14627

[15]*Southern Methodist University, Dallas, Texas 75275*
[16]*Syracuse University, Syracuse, New York 13244*
[17]*University of Texas - Pan American, Edinburg, Texas 78539*
[18]*Vanderbilt University, Nashville, Tennessee 37235*
[19]*Wayne State University, Detroit, Michigan 48202*
[20]*California Institute of Technology, Pasadena, California 91125*
[21]*University of California, Santa Barbara, California 93106*
[22]*Carnegie Mellon University, Pittsburgh, Pennsylvania 15213*
(Dated: July 23, 2002)

Abstract

With a sample of 9.7×10^6 $B\bar{B}$ pairs, CLEO has studied B decays to $\pi\ell\nu$, $\rho\ell\nu$, $\omega\ell\nu$, and $\eta\ell\nu$ where $\ell = e$ or μ, by incorporating the missing momentum into full B reconstruction. With the B^0 and B^+ modes combined according to isospin predictions for the relative partial widths, we obtain the preliminary results $\mathcal{B}(B^0 \to \pi^-\ell^+\nu[0 \le q^2 < 8\,\mathrm{GeV}^2]) = (0.427 \pm 0.109\ ^{+0.046}_{-0.051} \pm 0.006 \pm 0.016 \pm 0.001) \times 10^{-4}$, $\mathcal{B}(B^0 \to \pi^-\ell^+\nu[8 \le q^2 < 16\,\mathrm{GeV}^2]) = (0.687 \pm 0.107\ ^{+0.082}_{-0.089} \pm 0.008 \pm 0.036 \pm 0.008) \times 10^{-4}$, and $\mathcal{B}(B^0 \to \pi^-\ell^+\nu[q^2 \ge 16\,\mathrm{GeV}^2]) = (0.261 \pm 0.095\ ^{+0.046}_{-0.048} \pm 0.011 \pm 0.054 \pm 0.015) \times 10^{-4}$, which yield a total branching fraction of $\mathcal{B}(B^0 \to \pi^-\ell^+\nu) = (1.376 \pm 0.180\ ^{+0.116}_{-0.135} \pm 0.008 \pm 0.102 \pm 0.021) \times 10^{-4}$, where the errors are statistical, experimental systematic and the estimated uncertainties from the $\pi\ell\nu$ form factor, the $\rho\ell\nu$ form factors, and from modeling other $B \to X_u\ell\nu$ decays, respectively. We further obtain $|V_{ub}| = (3.25 \pm 0.21\ ^{+0.16}_{-0.18}\ ^{+0.64}_{-0.56} \pm 0.12 \pm 0.07) \times 10^{-3}$ by using various form factor predictions over the entire q^2 range from the pion mode. In a preliminary attempt to reduce modelling uncertainties, we extract $|V_{ub}|$ using a $\pi\ell\nu$ form factor from light cone sum rules in the range $q^2 < 16$ GeV^2 and from lattice QCD above this range and average the results to obtain $|V_{ub}| = (3.32 \pm 0.21\ ^{+0.17}_{-0.19}\ ^{+0.55}_{-0.39} \pm 0.12 \pm 0.07) \times 10^{-3}$. We do not extract a value for $|V_{ub}|$ from ρ information at this time. Finally, we find evidence for $\mathcal{B}(B^+ \to \eta\ell^+\nu) = (0.85 \pm 0.31 \pm 0.14) \times 10^{-4}$ (ISGW2 model) at a rate consistent, within sizable errors, with that expected from the measured pion rate and isospin relations. All results are preliminary.

*Submitted to the 31$^{\mathrm{st}}$ International Conference on High Energy Physics, July 2002, Amsterdam

I. INTRODUCTION

The element V_{ub} of the Cabbibo-Kobayashi-Maskawa (CKM) matrix [1] remains one of the most poorly constrained parameters of that matrix. Its magnitude, $|V_{ub}|$, plays a central role in constraints based upon the unitarity of the CKM matrix and inputs from both CP–conserving processes in the B meson decay and CP–violating processes in the neutral kaon and B systems. The value of $|V_{ub}|$ and, in particular, the accuracy to which we have measured this important parameter have been the subject of considerable debate over the past decade [2]. An accurate determination of $|V_{ub}|$ with well-understood uncertainties remains one of the fundamental priorities for heavy flavor physics.

A number of $|V_{ub}|$ measurement approaches have been attempted, and are reviewed in reference [2]. Inclusive techniques are hampered by a mismatch in kinematic regions where the large experimental backgrounds from $b \to c\ell\nu$ can be suppressed versus regions in which the theoretical uncertainties can be reliably determined. For exclusive reconstruction of particular final states, the primary challenge is calculation of the form factors for those channels. The first measurements of exclusive charmless semileptonic branching fractions [3], including evaluation of $|V_{ub}|$, were performed by the CLEO experiment at the Cornell Electron Storage Ring (CESR) using the modes $B^0 \to \pi^-\ell^+\nu$, $B^+ \to \pi^0\ell^+\nu$, $B^0 \to \rho^-\ell^+\nu$, $B^+ \to \rho^0\ell^+\nu$, $B^+ \to \omega\ell^+\nu$ and charge conjugate decays, where $\ell = e$ or μ. A second measurement of the $\rho\ell\nu$ modes by CLEO [4] using similar techniques but a much different signal to background optimization provided consistent, essentially independent, results with a similar total uncertainty. The combined analyses yielded $|V_{ub}| = (3.25 \pm 0.14^{+0.21}_{-0.29} \pm 0.55) \times 10^{-3}$. The π and ρ modes contribute about equally to this result.

This analysis presents an update by CLEO of the original exclusive $b \to u\ell\nu$ analysis [3], and is based on a total data sample of 9.70×10^6 $B\bar{B}$ pairs collected on the $\Upsilon(4S)$ resonance. The results presented here supersede those from the original CLEO analysis. In addition to more data, the analysis has been modified to minimize uncertainties arising from the q^2–dependence of the form factors. Most notably, the lower bounds on the signal charged lepton momentum for both the pseudoscalar and the vector modes have been lowered, and the branching fractions are determined independently in three q^2 regions. For the ρ modes, the branching fractions as a function of q^2 were first determined by the second CLEO $\rho\ell\nu$ analysis [4]. This analysis has a significantly broader accepted range for the charged lepton momentum, which in principle allows better discrimination among models.

II. EXCLUSIVE CHARMLESS SEMILEPTONIC DECAYS

The semileptonic transition of a B meson (a pseudoscalar) to a final state with a single pseudoscalar meson S can, in the limit of a massless charged lepton, be described by a single form factor $f_1(q^2)$:

$$\frac{d\Gamma(B^0 \to S^-\ell^+\nu)}{dy\, d\cos\theta_{W\ell}} = |V_{ub}|^2 \frac{G_F^2 k_S^3 M_B^2}{32\pi^3} \sin^2\theta_{W\ell} |f_1(q^2)|^2, \tag{1}$$

where $y = q^2/M_B^2$, k_S is the meson momentum and $\theta_{W\ell}$ is the angle between the charged lepton direction in the virtual W ($\ell + \nu$) rest frame and the direction of the virtual W. For a transition to a final state with a single vector meson P, three form factors A_1, A_2 and V

are necessary:

$$\frac{d\Gamma(B^0 \to P^- \ell^+ \nu)}{dy\, d\cos\theta_{W\ell}} = |V_{ub}|^2 \frac{G_F^2 k_P M_B^2 y}{128\pi^3} \times \tag{2}$$
$$\left[(1-\cos\theta_{W\ell})^2 \frac{|H_+|^2}{2} + (1+\cos\theta_{W\ell})^2 \frac{|H_-|^2}{2} + \sin^2\theta_\ell |H_0|^2\right],$$

where k_P is the meson momentum and the three helicity amplitudes are given by

$$H_\pm = \frac{1}{M_B + m_P}\left[A_1(q^2) \mp 2M_B k_P V(q^2)\right] \tag{3}$$
$$H_0 = \frac{1}{\sqrt{y}} \frac{M_B}{2m_P(M_B + m_P)} \left[\left(1 - \frac{m_P^2}{M_B^2} - y\right) A_1(q^2) - 4k_P^2 A_2(q^2)\right]. \tag{4}$$

The structure of these differential decay rates immediately allows us to draw some general conclusions regarding the properties of the semileptonic decays that we reconstruct in this analysis. For the $\rho(\omega)\ell\nu$ transitions, the left-handed, $V-A$, nature of the charged current at the quark level manifests itself at the hadronic level via $|H_-| > |H_+|$. The H_- contribution is also expected to dominate the H_0 contribution, leading to a forward-peaked distribution for $\cos\theta_{W\ell}$. For $\pi(\eta)\ell\nu$, there is clearly a $\sin^2\theta_{W\ell}$ dependence, independent of the form factor. The pseudoscalar modes also contain an extra factor of the meson momentum squared, which suppresses the rate near $q^2_{\max}$ ($p = 0$). Taken together these two effects give the pseudoscalar modes a softer momentum spectrum than the vector modes.

Calculation of the form factors has become a considerable theoretical industry, with a variety of techniques now being employed. Form factors based on lattice calculations[5]–[17] and on light cone sum rules[18]–[26] currently have uncertainties in the 15% to 20% range. A variety of quark model calculations exist[27]–[41]. Finally, a number of other approaches[42]–[47] such as dispersive bounds and experimentally–constrained models based on HQS all seek to improve the range of q^2 over which the form factors can be estimated without introduction of significant model dependence. Figure 1 illustrates the broad variation in shape that arises in the literature. Unfortunately, all the form factor calculations currently have contributions to the uncertainty that are uncontrolled. The light cone sum rules calculations assume quark–hadron duality, offering a "canonical" contribution to the uncertainty of 10%, but with no known means of rigorously limiting that uncertainty. The lattice calculations to date remain in the "quenched" approximation (no light quark loops in the propagators), which limits the ultimate precision to the 15% to 20% range. With the quark model calculations it is difficult to quantify the uncertainty of a particular calculation by their very nature of being a model. These uncertainties in the form factors translate directly into the same fractional uncertainty on $|V_{ub}|$.

III. EVENT RECONSTRUCTION AND SELECTION

The CLEO detector [48, 49] contains three concentric tracking devices within a 1.5 T superconducting solenoid that detect charged particles over 95% (93%) of the solid angle for the first 1/3 (last 2/3) of the data. For the last 2/3 of the data, a silicon vertex detector replaced a straw-tube wire chamber. The momentum resolution at 2 GeV/c is 0.6%. A CsI(Tl) electromagnetic calorimeter, also inside the solenoid, covers 98% of 4π. A typical

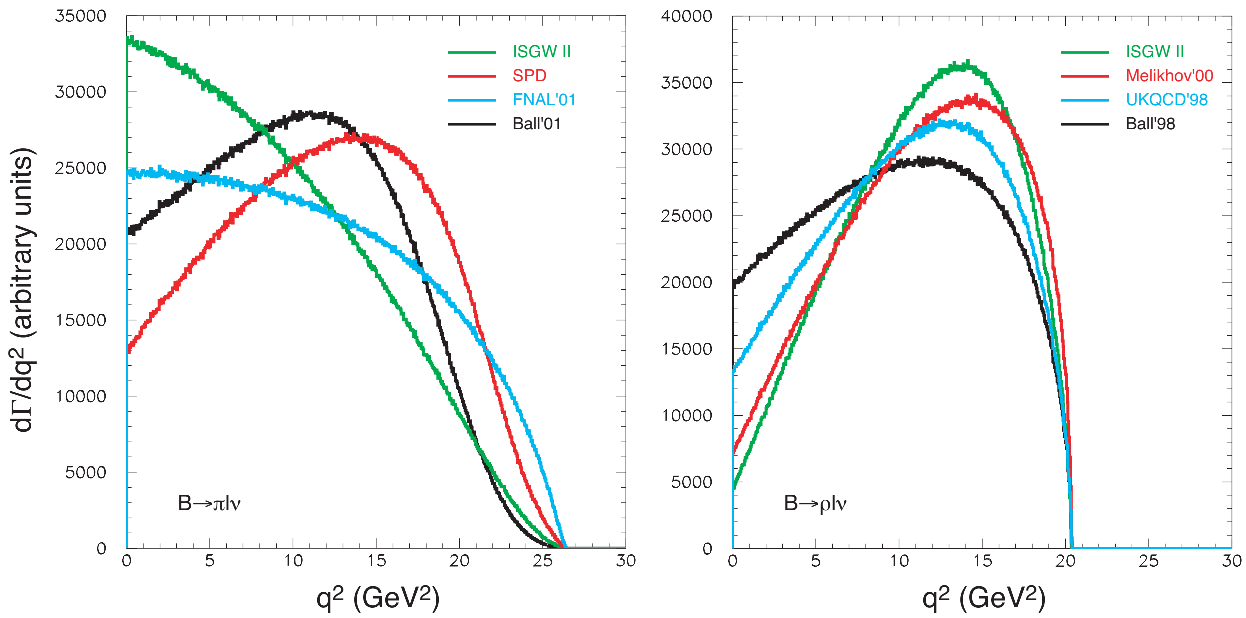

FIG. 1: Predictions for $d\Gamma(B \to \pi\ell\nu)/dq^2$ (left) and for $d\Gamma(B \to \rho\ell\nu)/dq^2$ (right) for a variety of models, illustrating the range of variation of the predicted q^2–dependence.

π^0 mass resolution is 6 MeV. Charged tracks are assigned the most probable mass based on specific ionization, time of flight, and the relative rates as a function of momentum for proton, K^+ and π^+ production in B decay.

The undetected neutrino complicates analysis of semileptonic decays. Because of CLEO's hermeticity, we can reconstruct the neutrino via the missing energy ($E_{\rm miss} \equiv 2E_{\rm beam} - \sum E_i$) and missing momentum ($\vec{P}_{\rm miss} \equiv -\sum \vec{p}_i$) in each event. In the process $e^+e^- \to \Upsilon(4S) \to B\bar{B}$, the total energy of the beams is imparted to the $B\bar{B}$ system; at CESR, that system is at, or nearly at, rest (a small crossing angle has been in use at CESR for most of the running). The neutrino combined with the signal lepton (ℓ) and meson (m) should thus satisfy the constraints on energy, $\Delta E \equiv (E_\nu + E_\ell + E_m) - E_{\rm beam} = 0$, and on momentum, $M_{m\ell\nu} \equiv [E^2_{\rm beam} - |\alpha\vec{p}_\nu + \vec{p}_\ell + \vec{p}_m|^2]^{\frac{1}{2}} = M_B$, where α is chosen to force $\Delta E = 0$. The neutrino momentum resolution dominates the ΔE resolution, so the momentum scaling corrects for the mismeasurement of the magnitude of the neutrino momentum in the $M_{m\ell\nu}$ calculation, leaving the neutrino direction as the dominant source of smearing in this mass calculation. Signal MC events have a $|\vec{P}_{\rm miss}|$ resolution of 85 MeV$/c$ after all cuts. Because the resolution on $E_{\rm miss}$ is about 3 times larger [50], we use $(E_\nu, \vec{p}_\nu) = (|\vec{P}_{\rm miss}|, \vec{P}_{\rm miss})$ to calculate ΔE and $M_{m\ell\nu}$. Significant effort has been devoted to minimize multiple counting of charged particles in the track reconstruction (*e.g.*, particles that curl multiple times within the tracking volume) and to suppress clusters in the calorimeter from charged hadrons that have interacted.

We reconstruct $q^2 = M^2_{W^*} = (p_\nu + p_\ell)^2$ for each decay from the reconstructed lepton four momentum and the missing momentum. In addition to using the scaled reconstructed momentum $\alpha\vec{p}$ described above, the direction of the missing momentum is changed through the smallest angle consistent with forcing $M_{m\ell\nu} = M_B$. This procedure results in a q^2 resolution of 0.31 GeV^2. The $\pi\ell\nu$ and the $\rho\ell\nu$ modes are analyzed separately in the intervals $q^2 < 8$ GeV^2, $8 \leq q^2 < 16$ GeV^2 and $q^2 \geq 16$ GeV^2. For the $\omega\ell\nu$ and $\eta\ell\nu$ modes, which have low statistics, we do not bin in q^2.

Information from specific ionization is combined with calorimetric and tracking measurements to identify electrons with $p > 600$ MeV/c over 90% of the solid angle. Particles registering hits in counters deeper than 5 interaction lengths over the polar angle range $|\cos\theta| < 0.85$ are considered muons. Those with hits beyond 3 interaction lengths over $|\cos\theta| < 0.71$ are used in a multiple-lepton veto, described below. Candidate leptons must have $p_\ell > 1.0$ GeV/c for the π and η modes and $p_\ell > 1.5$ GeV/c for the ρ and ω (vector) modes, which can couple to the W helicities ± 1 and hence have a harder spectrum. The identification efficiency above 1.5 GeV/c averages over 90%; the probability that a hadron is misidentified as an electron (muon), a "fake lepton", is about 0.1% (1%).

The 5 interaction length requirement for muons causes the muon acceptance to fall rapidly below 1.4 GeV/c. As a result, only electrons contribute at the low end of the momentum range we accept for $\pi\ell\nu$, and electrons dominate the measurement in the lowest q^2 interval.

A π^0 candidate must have a $\gamma\gamma$ mass within 2 standard deviations of the π^0 mass. We study the ω via its $\pi^+\pi^-\pi^0$ decay; we reduce combinatoric background by rejecting combinations away from the center of the ω Dalitz plot. We reconstruct η in both the $\gamma\gamma$ and the $\pi^+\pi^-\pi^0$ decay modes. For the $\gamma\gamma$, we require the reconstructed mass to be within 2 standard deviations of the η mass (within about 26 MeV). For the $\pi^+\pi^-\pi^0$, we require $|m_{\pi^+\pi^-\pi^0} - m_\eta| < 10$ MeV (about 1.7 times the resolution).

Backgrounds arise from the $e^+e^- \to q\bar{q}, \tau^+\tau^-$ continuum, fake leptons, $b \to c\ell\nu$, and other $b \to u\ell\nu$ modes. Backgrounds from continuum processes are suppressed by use of two event shape variables. The first variable is the angle ($\cos\theta_{thrust}$) between the thrust axis evaluated for the signal mode particles (not including the neutrino) and that for the rest of the event. For $B\bar{B}$ events at CESR, this angle is flat because the decay orientations for each B are independent and the B's are nearly at rest, while for continuum the angle is strongly forward and backward peaked. The ratio ($R2$) of the second to the zeroth Fox-Wolfram moment [51], which distinguishes spherical from jetty topologies, is also utilized. The continuum background tends to have a small reconstructed q^2. We therefore tune the continuum cut employed in the $R2$–$\cos\theta_{thrust}$ plane for each q^2 interval separately in the π and the ρ modes. For the ω and η modes, for which all q^2 regions are combined, only a $\cos\theta_{thrust}$ cut is applied to reduce uncertainties from the q^2–dependence of the form factors. Signal events with low q^2 appear rather jetty, so a cut using $R2$, when data is binned over a broad q^2 range, would introduce an efficiency bias. These criteria suppress the continuum background by over a factor of 10 and are about 80% efficient.

The $|p_\ell|$ cuts greatly reduce background from $b \to c \to s\ell\nu$ and bias mildly against $b \to c\ell\nu$. In the vector modes, we further require $\cos\theta_{W\ell} > 0$ since the signal rate is largely suppressed by $V - A$ outside this region, while the background is roughly flat in the region excluded, and falls off in the region accepted.

All criteria were studied with background and signal Monte Carlo (MC), not data, to avoid potential biases.

Backgrounds, particularly $b \to c\ell\nu$, can smear into the signal (ΔE,$M_{m\ell\nu}$) region when $\vec{P}_{\rm miss}$ misrepresents $\vec{p}_\nu$. Such backgrounds are highly suppressed by rejecting events with multiple leptons or a total charge $|\Delta Q| > 1$, both of which indicate missing particles, or with $M^2_{\rm miss} \equiv E^2_{\rm miss} - |\vec{P}_{\rm miss}|^2$ inconsistent with zero. Still, Monte Carlo studies show that the dominant remaining $b \to c\ell\nu$ events contain either a K_L or second neutrino (from $c \to s\ell\nu$ with the lepton not identified) that is roughly collinear with the primary neutrino.

IV. EXTRACTION OF BRANCHING FRACTIONS

We use a binned maximum likelihood fit to extract the rates, binning the data in each mode coarsely over the region ($5.175 \leq M_{m\ell\nu} < 5.2875$ GeV, $|\Delta E| < 0.75$ GeV). The choice of binning balanced separation of signal and background against reliance on detailed MC shape predictions. To examine yields, efficiency and kinematics, we use the most sensitive bin (the "signal bin") $5.265 \leq M_{m\ell\nu} < 5.2875$ GeV and $-0.15 \leq \Delta E < 0.25$ GeV, though neighboring bins also contribute information to the fit. For comparison, the ΔE and $M_{m\ell\nu}$ resolutions are about 100 MeV and 7 MeV, respectively, dominated by the resolution on $|\vec{p}_\nu|$. In the $\rho\ell\nu$ ($\omega\ell\nu$) modes, we further divide the yields into three equal bins over the $\pi\pi$ (3π) mass range within ± 285 MeV (± 30 MeV) of the nominal ρ (ω) mass. The 2π (or 3π) mass intervals ± 95 MeV and ± 10 MeV are used for figures for ρ and ω candidates, respectively. We bin the $|\Delta Q| = 1$ and $|\Delta Q| = 0$ separately, taking advantage of the better signal to noise ratio of the $|\Delta Q| = 0$ sample but still reducing our dependence on our knowledge of the absolute tracking efficiency.

We do not use information from the lepton momentum spectrum or from $\cos\theta_{W\ell}$ within the fit to help minimize the model dependence of the branching fraction determinations.

To simplify the statistical interpretation of the results, we limit the number of multiple entries per event. For each individual mode, the candidate with smallest $|\Delta E|$ among those satisfying $M_{m\ell\nu} > 5.175$ GeV is chosen, independent of q^2. A given event can contribute to multiple modes, though contribution near the signal region in more than one mode is rare. In the ρ and ω modes, each mass bin above is considered a separate mode.

MC simulation provided the distributions in each mode for signal, the $b \to c$ background, the crossfeed among the modes, and the feeddown from higher mass $B \to X_u\ell\nu$ decays. It included a full description of the $b \to c$ and charm decay modes and a GEANT-based [52] detector model. The $X_u\ell\nu$ feeddown was evaluated with a simulation of the $B \to X_u\ell\nu$ process using an inclusive calculation [53] of $d\Gamma(B \to X_u\ell\nu)/dM_{X_u}$ with parameters from the CLEO analysis of the $B \to X_s\gamma$ photon spectrum [54, 55] used in the recent CLEO lepton momentum endpoint analysis [56]. The nominal analysis married this inclusive spectrum to the ISGW II model [30] for all mesons through the $\rho(1450)$ by "subtracting rate" from the inclusive calculation with a weighting like $\exp{(M_{X_u} - M_R)^2/\Lambda^2_{QCD}}$, where M_R is the central mass of the resonance R. At any given M_{X_u}, the rate remaining after this subtraction of the exclusive modes is hadronized nonresonantly. Variations of the inclusive parameters based on the uncertainties in the $B \to X_s\gamma$ analysis and variations of the hadronization model (*e.g.*, fully nonresonant but with $\pi\pi\ell\nu$ removed from the ρ mass region) are included in the systematic uncertainties. The signal modes are excluded from these $B \to X_u\ell\nu$ samples.

The contributions from events in which hadrons have faked the signal leptons and from continuum are evaluated using data. The electron and muon identification fake rates from pions, kaons and protons are measured in data using a variety of tagged samples. The analysis is performed on a sample of hadronic events with no identified leptons, treating each track in turn as a signal electron and then a signal muon and the contribution in each mode is weighted according to the fake rate.

We determined the residual continuum background using data collected 60 MeV below the $\Upsilon(4S)$ energy. The center of mass energy and cross section differences were taken into account as necessary. To smooth the statistical fluctuations within this sample, we obtain a high statistics off-resonance sample by removal of the continuum suppression sample, but with all other cuts remaining the same. We use continuum MC, $\tau^+\tau^-$ MC and our fake-

TABLE I: The efficiency matrix in percent describing the probability that an event from a given generated q^2 interval reconstructs in a given q^2 interval for $B^0 \to \pi^- \ell^+ \nu$ events that pass all cuts and reconstruct within the "signal region" of ΔE versus $M_{m\ell\nu}$. The efficiencies are based on Ball'01.

true q^2	reconstructed q^2		
(GeV^2)	$0-8$	$8-16$	≥ 16
$0-8$	2.461	0.067	0.001
$8-16$	0.068	4.570	0.064
≥ 16	0.000	0.150	4.387

lepton samples to estimate biases in the distribution of data in the ΔE versus $M_{m\ell\nu}$ plane for each combination of mode, reconstructed q^2 bin, and for $\Delta Q = 0$versus $|\Delta Q| = 1$. This bias is applied to the sample without standard continuum suppression applied, and the resulting ΔE versus $M_{m\ell\nu}$ distributions normalized to the corresponding distributions with the suppression applied.

For each signal mode, we generate a sample of signal Monte Carlo that is flat in phase space and feed these samples to our GEANT-based detector simulation. At analysis time, we reweight these events to correspond to a particular calculation of for the form factors involved in the decays. This allows us to sample a variety of calculations. For each mode, we determine the efficiency matrix for reconstructed versus true q^2. Given our resolution and binning, the matrix is essentially diagonal, as Table I shows for the form factor calculation of Ball and Zwicky (Ball'01) [26].

We fit the six modes, the two η submodes and the separate q^2 bins simultaneously. The signal rates for each q^2 range float separately. The isospin and quark symmetry relations $\Gamma(B^0 \to \pi^- \ell^+ \nu) = 2\Gamma(B^+ \to \pi^0 \ell^+ \nu)$ and $\Gamma(B^0 \to \rho^- \ell^+ \nu) = 2\Gamma(B^+ \to \rho^0 \ell^+ \nu) = 2\Gamma(B^+ \to \omega \ell^+ \nu)$ constrain the rates for B^+ relative to B^0, and are assumed to hold for each q^2 region. For the reconstructed ω mode, the $\omega\ell^+\nu$ yields from each q^2 range are combined for each iteration of the fit according to the above constraints to provide the rates for that mode. Hence we fit for three independent $\pi^\pm \ell^\mp \nu$ yields and three independent $\rho^\pm \ell^\mp \nu$ yields. A single $\eta\ell\nu$ branching fraction is fit for, with the relative branching fractions and efficiencies transforming this rate into those needed for the two submodes. To implement the isospin constraints, we assume equal charged and neutral B production, $f_{+-} = f_{00}$, and input a lifetime ratio of 1.062 ± 0.029 [57]. For self-consistency, the crossfeed rates are constrained to the observed yields.

The $b \to c$ normalization in the fit varies independently for each mode, and within each mode for $\Delta Q = 0$ and $|\Delta Q| = 1$. The normalizations obtained are generally within 10% of those derived from luminosity and cross sections.

We do not float the normalization of the generic $B \to X_u \ell\nu$ feeddown sample in the fit, aside from systematic checks. We calculate a scale factor for the feeddown sample so that the branching fraction in the $2.2-2.6$ GeV lepton momentum range that we obtain from the sum of the contributions from all q^2 regions from all signal modes and from the feeddown sample matches that recently measured by CLEO [56]. We iterate the fitting procedure, updating the branching fractions from each previous fit and extracting a new scale factor until the process converges. The systematic error evaluation and checks using alternate procedures are described below. This iterative procedure is repeated for any variation in the various Monte Carlo, continuum or fake samples described below.

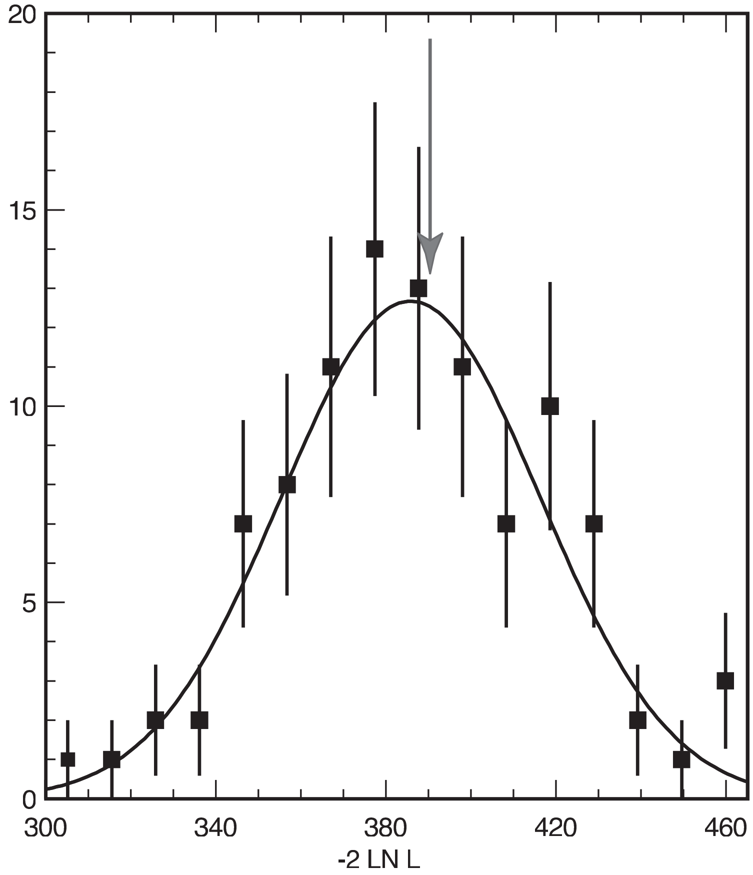

FIG. 2: Distribution of $-2\ln L$ from the bootstrap procedure described in the text. The arrow indicates the value obtained from the nominal fit.

We extend the likelihood method to include the finite statistics of the Monte Carlo, off-resonance and fake lepton samples following the method of Barlow and Beeston [58].

For these preliminary results, we have examined the following form factor for the signal modes and crossfeed rates. For $\pi\ell\nu$: Ball and Zwicky (light cone sum rules) [26], ISGW II (a nonrelativistic quark model), and the skewed parton distributions (SPD) of Feldmann and Kroll [38]. Lattice and other LCSR calculations will also be considered in the final results. For $\rho\ell\nu$: Ball and Braun (light cone sum rules – Ball'98) [19], ISGW II, Melikhov and Stech (a relativistic quark model – Melikhov'00) [37] and UKQCD (a lattice QCD calculation – UKQCD 98) [7]. For $\eta\ell\nu$, we have only considered the ISGW II form factor to date. For nominal yields and figures, we use Ball'01 for the π modes and Ball'98 for the vector modes. From the nominal fit we obtain a value $-2\ln L = 390.5$ for 385 degrees of freedom.

We have examined the reliability of our fitting procedure via a bootstrap technique. We created 100 mock data samples by randomly choosing a subset of events from each of our Monte Carlo samples. From fits to these samples we find that our procedure reproduces the branching fractions without bias, and that the scatter of central values agrees with the uncertainties reported by the fit to better than 15%. The distribution of likelihoods and that obtained from our nominal fit are shown in Figure 2. The result from the fit to data is reasonable. Most bins in the data fit have sizable statistics, so interpretation of $-2\ln L$ as a χ^2 is reasonable. The probability of χ^2 for the nominal fit to the data is 0.41.

In Figures 3 through 6 we show the $M_{m\ell\nu}$ (ΔE) distributions in the ΔE ($M_{m\ell\nu}$) signal

TABLE II: Summary of branching fractions corresponding to yields in the $(\Delta E, M_{m\ell\nu})$ signal bin from the nominal fit using the Ball'01 and Ball'98 form factors for the π and ρ modes, respectively. The first uncertainties are statistical and the second systematic.

Mode	q^2 interval (GeV^2)	$\mathcal{B} \times 10^4$
$B^0 \to \pi^- \ell^+ \nu$	$\mathcal{B}_{\text{total}}$	$1.376 \pm 0.180\ ^{+0.117}_{-0.136}$
	$\mathcal{B}_{<8}$	$0.427 \pm 0.109\ ^{+0.046}_{-0.051}$
	$\mathcal{B}_{8-16}$	$0.687 \pm 0.107\ ^{+0.082}_{-0.089}$
	$\mathcal{B}_{\geq 16}$	$0.261 \pm 0.095\ ^{+0.048}_{-0.050}$
$B^0 \to \rho^- \ell^+ \nu$	$\mathcal{B}_{\text{total}}$	$1.985 \pm 0.284\ ^{+0.633}_{-0.691}$
	$\mathcal{B}_{<8}$	$0.460 \pm 0.186\ ^{+0.358}_{-0.363}$
	$\mathcal{B}_{8-16}$	$1.000 \pm 0.199\ ^{+0.460}_{-0.481}$
	$\mathcal{B}_{\geq 16}$	$0.525 \pm 0.083\ ^{+0.109}_{-0.131}$
$B^+ \to \eta \ell^+ \nu$	$\mathcal{B}_{\text{total}}$	$0.849 \pm 0.309\ ^{+0.138}_{-0.144}$

band for the individual q^2 regions examined for $\pi\ell\nu$ and for $\rho\ell\nu$. The fits describe the data in these regions quite well. The distributions summed over q^2 for the π and ρ modes and for $\omega\ell\nu$ and $\eta\ell\nu$ are shown in Fig. 7. The $\omega\ell\nu$ mode remains consistent both with the level expected given the $\rho\ell\nu$ rate and with pure background.

The lepton momentum spectra for events in the $(M_{m\ell\nu}, \Delta E)$ signal bin are shown in Figures 8 and 9. This information is not used in the fit, but shows good agreement with the signals preferred in the fit.

The branching fractions from the nominal fit are summarized in Table II.

The increase in $-2\ln\mathcal{L}$ from best fit to $\mathcal{B}(B \to \eta\ell\nu) = 0$ is 11.8, corresponding roughly to a 3.4σ statistical significance.

V. EXPERIMENTAL SYSTEMATICS

Table III summarizes the contributions to the systematic errors. Uncertainty in the decay model of the nonsignal B and inaccuracies in detector simulation constitute the dominant contributions. We investigated many of the effects of misreconstruction on the neutrino reconstruction and associated event selection by modifying the reconstruction output of all of the Monte Carlo samples used in the fit. Using independent studies by CLEO for this and other analyses, our modifications reflected the uncertainties in charged particle and photon-finding efficiencies, simulation of false charged particles and photons, charged particle momentum resolution, photon energy resolution, hadronic shower simulation and charged particle identification. The full MC samples were re-analyzed for each variation to allow for leakage of events across the selection boundaries. In addition, we reweighted the Monte Carlo samples to account for the uncertainties in the rate and spectrum for K_L^0 production in B decay and in the process $b \to c \to s\ell\nu$, both of which affect the background rate into the signal region.

We reweight the Monte Carlo to allow variation in the relative rates for $D^*\ell\nu$, $D\ell\nu$, $(Dn\pi)_{resonant}\ell\nu$ and $(Dn\pi)_{nonresonant}\ell\nu$. We vary the rates by $\pm 8\%$, $\pm 6\%$, $\pm 31\%$ and $\pm 29\%$, respectively. Note that if we completely eliminate any of these charmed modes except $D^*\ell\nu$, the total branching fractions for π and ρ remain stable within 4% of themselves, which demonstrates that we are quite insensitive to the details of the poorly measured nonresonant

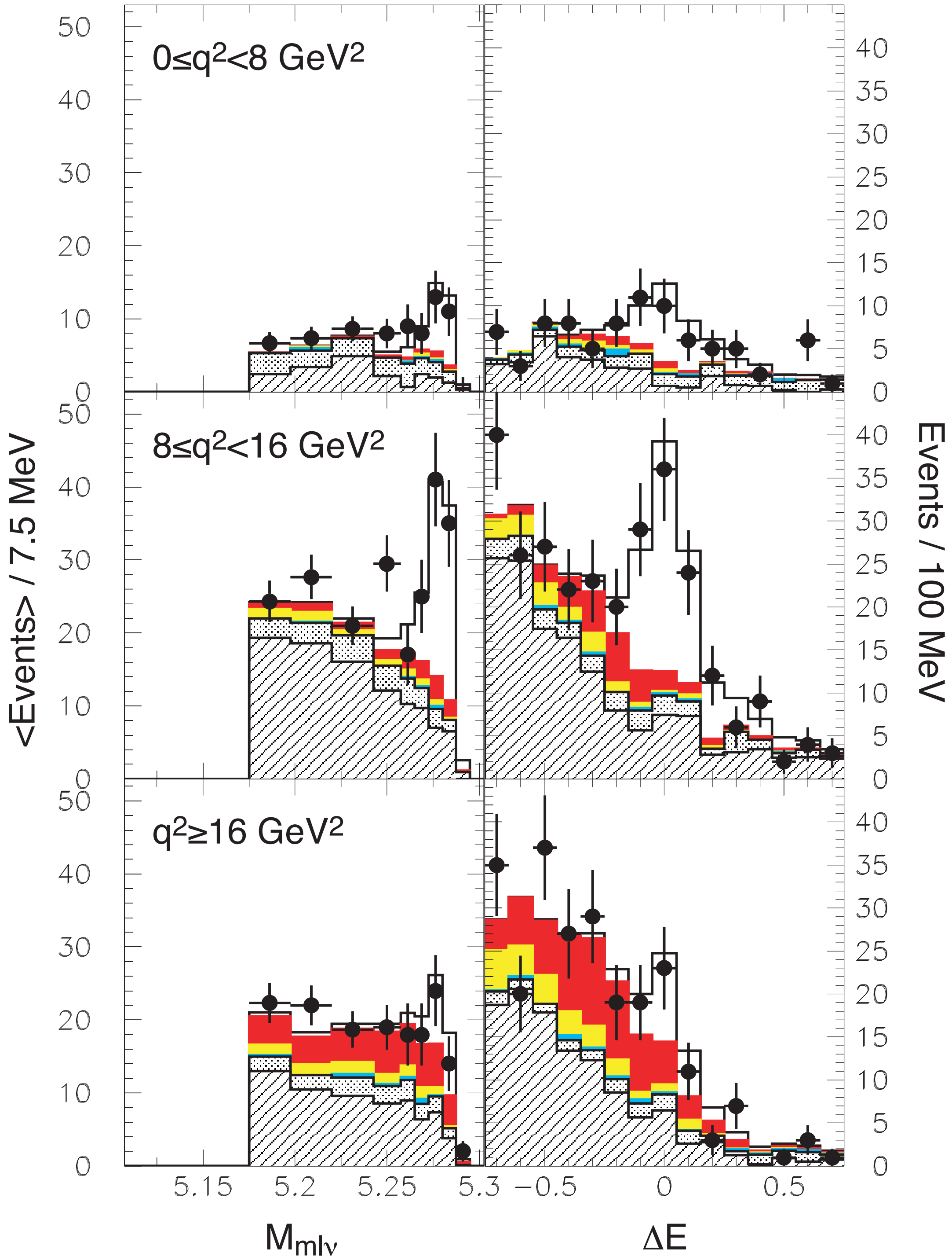

FIG. 3: $M_{m\ell\nu}$ (left) and ΔE (right) in the ΔE and $M_{m\ell\nu}$ "signal" band requiring $\Delta Q = 0$ for the combined $\pi^{\pm}, \pi^0$ modes. The points are the on-resonance data. The histogram components, from bottom to top, are $b \to c$ (hatched), continuum (dotted), fake leptons (cyan or dark grey), feeddown from other $B \to X_u \ell\nu$ modes (yellow or light grey), cross feed from other signal modes into the reconstructed modes (red or black) and signal (open). The normalizations are from the nominal fit.

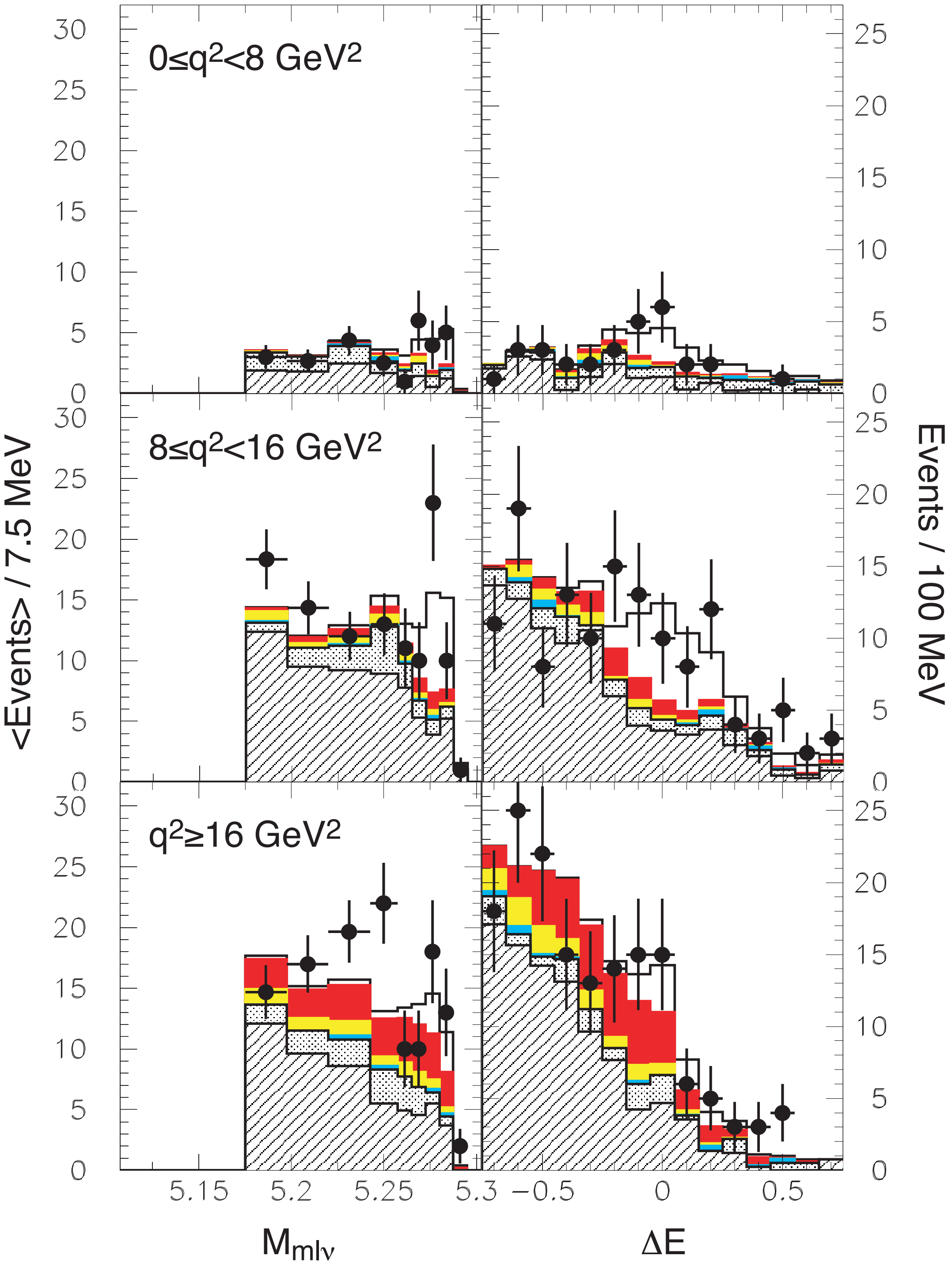

FIG. 4: $M_{m\ell\nu}$ (left) and ΔE (right) in the ΔE and $M_{m\ell\nu}$ "signal" band requiring $|\Delta Q| = 1$ for the combined $\pi^{\pm}, \pi^0$ modes. The points are the on-resonance data. See Fig. 3 for component and normalization descriptions.

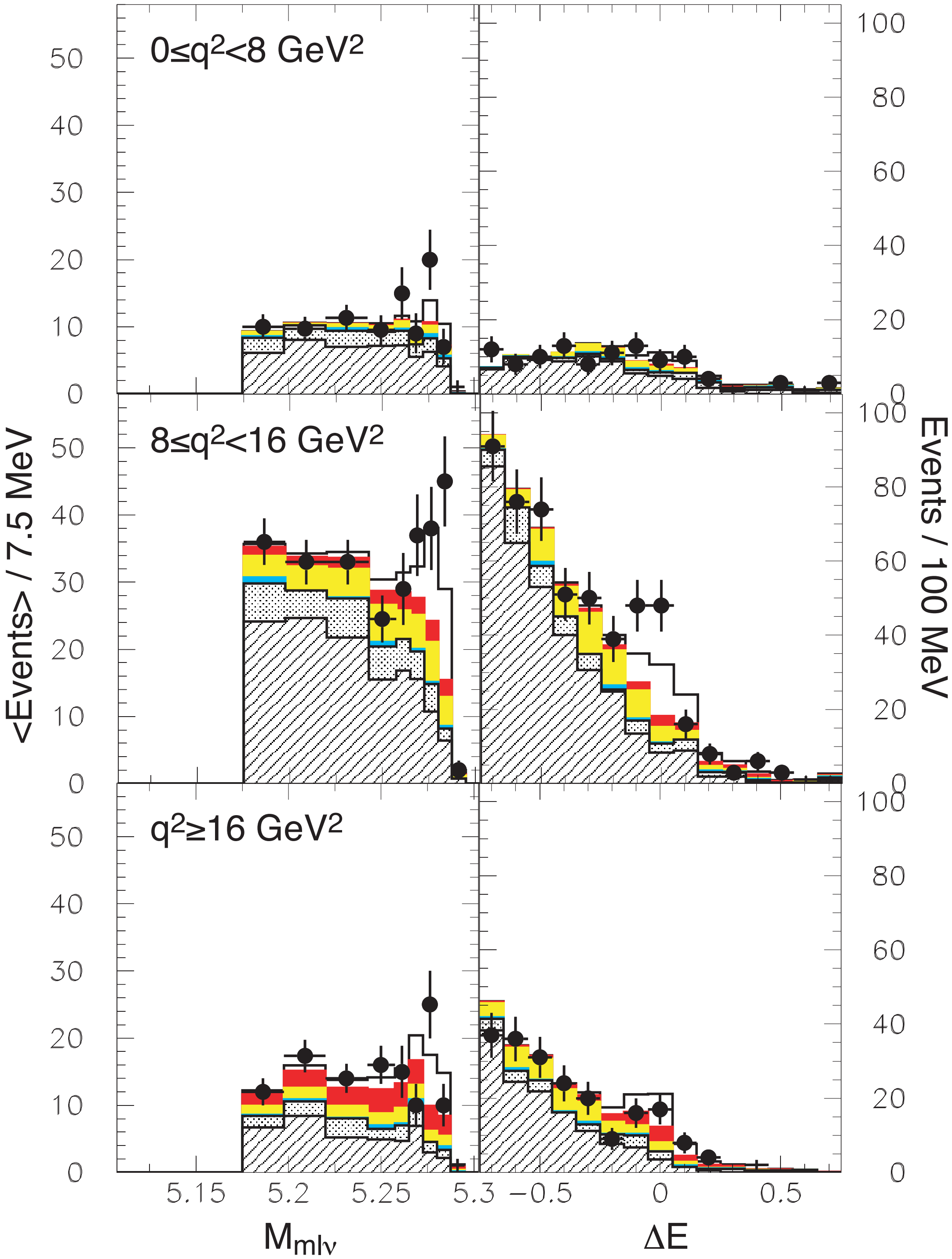

FIG. 5: $M_{m\ell\nu}$ (left) and ΔE (right) in the ΔE and $M_{m\ell\nu}$ "signal" band requiring $\Delta Q = 0$ for the combined $\rho^{\pm}, \rho^0$ modes. The points are the on-resonance data. See Fig. 3 for component and normalization descriptions.

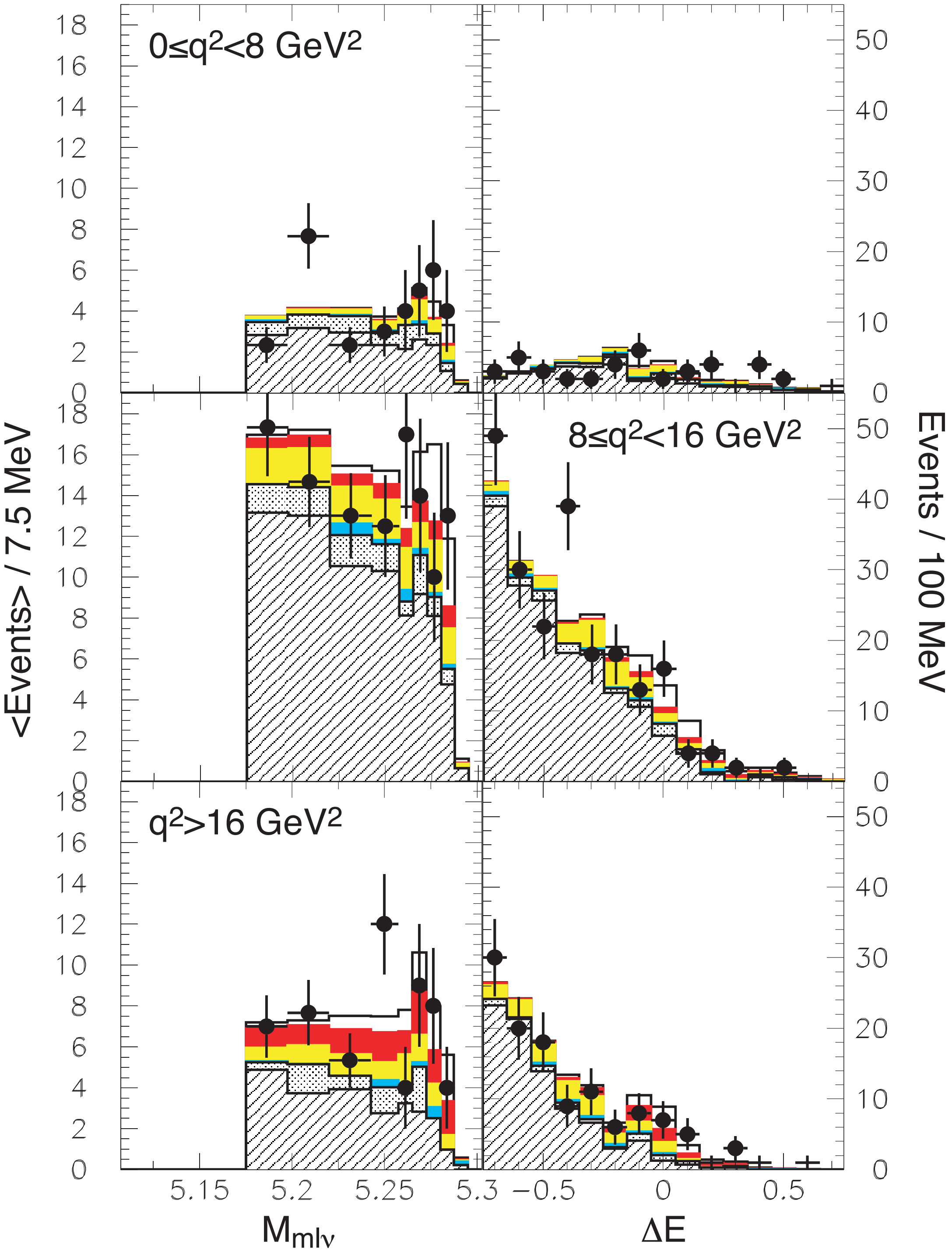

FIG. 6: $M_{m\ell\nu}$ (left) and ΔE (right) in the ΔE and $M_{m\ell\nu}$ "signal" band requiring $|\Delta Q| = 1$ for the combined $\rho^{\pm}, \rho^0$ modes. The points are the on-resonance data. See Fig. 3 for component and normalization descriptions.

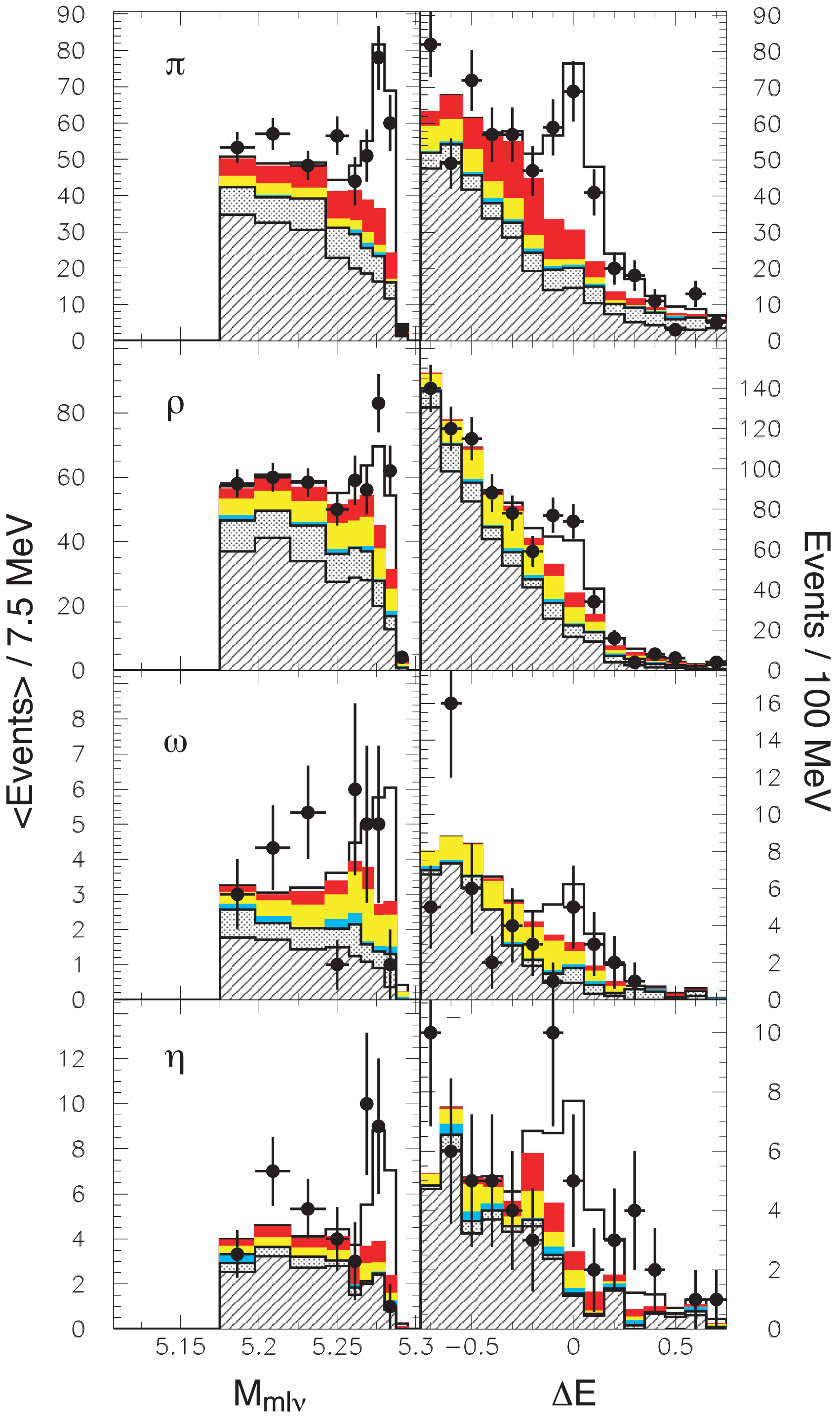

FIG. 7: $M_{m\ell\nu}$ (left), ΔE (right) in the ΔE and $M_{m\ell\nu}$ signal bands for $\Delta Q = 0$ and summed over the entire q^2 range for the combined π modes (top), ρ modes (row 2), ω (row 3) and η (bottom) modes. See Fig. 3 for component and normalization description.

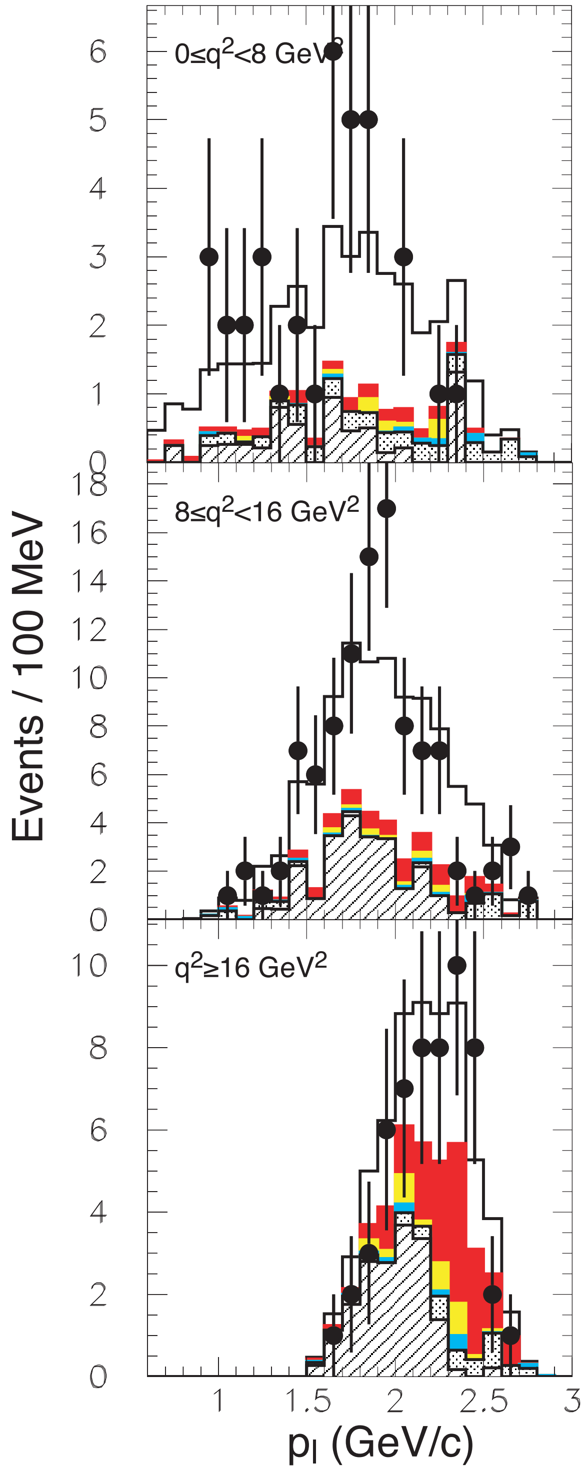

FIG. 8: Charged lepton momentum spectrum for the combined $\pi\ell\nu$ modes in the three q^2 intervals. See Fig. 3 for component and normalization descriptions.

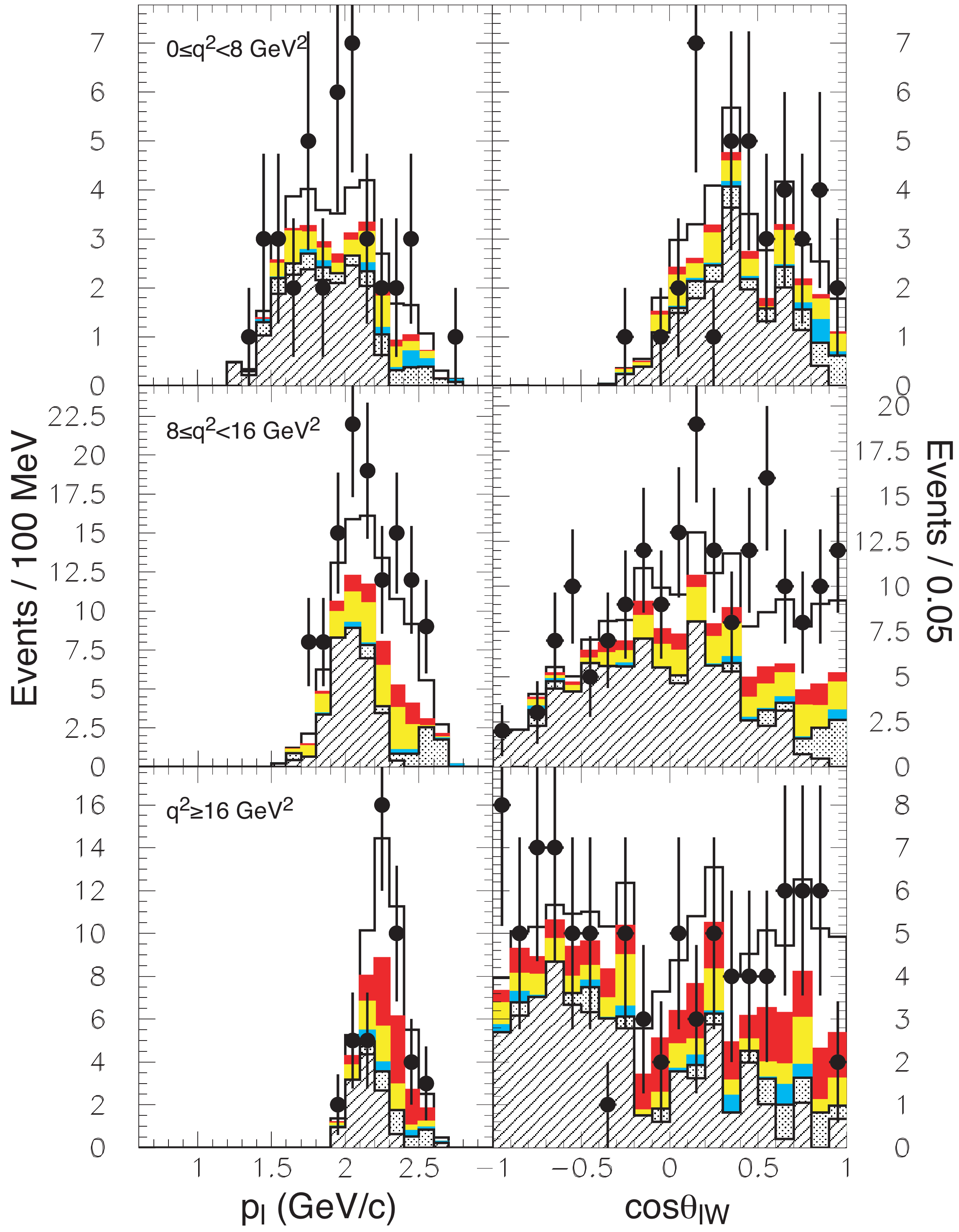

FIG. 9: Charged lepton momentum spectrum (left) and $\cos\theta_{W\ell}$ (right) for the combined $\rho\ell\nu$ modes in the three q^2 intervals. See Fig. 3 for component and normalization descriptions.

and resonant ($Dn\pi$) modes. For $\pi\ell\nu$, zeroing $D^*\ell\nu$ caused only a 14% change.

As mentioned above, we vary the nonperturbative parameters of the inclusive spectrum used to drive the $X_u\ell\nu$ simulation within the uncertainties obtained from the $B \to X_s\gamma$ analysis that were used in the recent endpoint measurement [55, 56]. We have also tried a strictly resonant description of ISGW II. For each of the sets of nonperturbative parameters, we examine the nominal hadronization model described above and a completely nonresonant model (with a variety of mass cuts to eliminate effective overlap with the signal modes). Finally, we vary the normalization of the $X_u\ell\nu$ background sample by having the endpoint branching fraction in the iterative fit procedure converge to the ± 1 sigma variations of the measured endpoint branching fraction [56]. In addition to these variations, which form the basis of the systematic uncertainty estimates, we have checked the results using alternate procedures for handling of the $X_u\ell\nu$ background. We have let the normalization float in the fit. We have let the normalizations for the background to $\pi\ell\nu$, to $\rho\ell\nu$, and to the other modes float independently. We have let the normalization float, but with the addition of a χ^2 term to the likelihood to constrain the deduced endpoint branching fraction to agree with the experimental result [56] within the measured uncertainties. These checks are consistent within the systematic uncertainty assigned.

For many of the variations, we expect a cancellation in the change in the yield and the change in the efficiency. If we degrade the neutrino, the efficiency for signal is reduced, but background tends to smear more readily into the signal region. Hence the signal yield also tends to be reduced, offsetting the change in efficiency. Because of the expected imperfections in our simulation, we do not expect the observed cancellation to be perfectly reliable. For each variation, we therefore assign an uncertainty in the branching fraction to be

$$\sigma = \sigma_{BR} \oplus \frac{\sqrt{2}}{3} \min(\sigma_{yield}, \sigma_{eff}), \tag{5}$$

where σ_{BR} is the percentage change in the branching fraction from the fit, σ_{yield} is the percentage change in the "signal bin" yield, and σ_{eff} is the percentage change in the "signal bin" efficiency. For complete cancellation ($\sigma_{yield} = \sigma_{eff}$; $\sigma_{BR} = 0$), the additional term amounts to the addition in quadrature of one third the change observed in the yield and in the efficiency. When no cancellation is expected, the additional term is zero.

For each test summarized above, we have repeated our iterative fitting procedure until the fits and scale factor for $B \to X_u\ell\nu$ converge to yield the measured endpoint rate. As Table III shows, the $\pi\ell\nu$ and $\eta\ell\nu$ results are stable under these variations. For the $\rho\ell\nu$ rate, however, we see significant variation.

In the ρ modes, there is an additional uncertainty from the unknown contribution of nonresonant $\pi\pi\ell\nu$ decays. The uncertainty from this background was limited in the previous analysis by use of reconstructed $\pi^0\pi^0\ell^\pm\nu$ decays. In this analysis, the uncertainty should be reduced because of the increased statistical precision. We have not yet completed this study, so we have used the uncertainty estimate from the previous analysis.

In addition to the variations above, we have performed various systematic checks, including variation of the selection criteria and investigation of electron and muon samples separately. The observed variations were in general consistent within the uncertainties resulting from the statistical changes.

Use of a χ^2–based fitting procedure produced similar results, though we see that low statistics bins clearly have an undue influence on the results of this fitter. Such sensitivity is eliminated with the log likelihood minimization.

TABLE III: Contributions to the systematic error (%) in each total and partial branching fraction ($\mathcal{B}$). Simulation of the detector and the second B contribute to ν simulation.

	$\pi\ell\nu$				$\rho(\omega)\ell\nu$				
		q^2 interval (GeV^2)				q^2 interval (GeV^2)			
Systematic	$\mathcal{B}_{\text{total}}$	< 8	$8-16$	≥ 16	$\mathcal{B}_{\text{total}}$	< 8	$8-16$	≥ 16	η
ν simulation	6.6	9.1	10.8	16.5	21.5	67.2	37.8	14.1	13.6
$B \to D/D^*/D^{**}/D^{\text{NR}}X\ell\nu$	1.7	2.5	1.9	3.2	2.0	21.4	4.7	4.2	5.5
$b \to u\ell\nu$ feeddown	1.5	0.2	1.1	5.6	22.7	30.5	25.2	13.5	2.8
Continuum smoothing	1.0	2.0	0.2	2.0	3.0	10.0	1.0	2.0	2.0
Fakes	3.0	3.0	3.0	3.0	3.0	3.0	3.0	3.0	3.0
f_{+-}/f_{00}	2.4	2.6	2.3	2.2	0.0	2.5	1.0	0.1	4.1
τ_{B^+}/τ_{B^0}	0.2	0.1	0.3	0.5	2.1	4.2	1.4	2.1	1.4
Isospin	0.0	0.0	0.0	0.2	2.4	1.9	2.7	2.3	0.1
Lepton ID	2.0	2.0	2.0	2.0	2.0	2.0	2.0	2.0	2.0
Luminosity	2.0	2.0	2.0	2.0	2.0	2.0	2.0	2.0	2.0
Upper	**8.5**	10.8	12.0	18.4	**31.9**	77.8	46.0	20.7	**16.2**
Non Resonant	-5	-5	-5	-5	-14	-14	-14	-14	-5
Lower	**9.9**	11.9	13.0	19.1	**34.8**	79.0	48.1	25.0	**17.0**

VI. FORM FACTOR DEPENDENCE

In the original measurement of the exclusive charmless branching fractions [3], there were two roughly comparable contributions to the branching fraction errors from the form factor uncertainties. The first component is induced when the efficiency varies as a function of q^2 (inescapable with a lepton momentum cut), and the data are binned over a broad range of q^2. Because we extract the rates independently in three separate q^2 ranges, this analysis should see a significant reduction from this effect. The second contribution results because there is significant q^2 dependence to the crossfeed rates between the pseudoscalar and the vector modes. Again, since we extract the rates independently as a function of q^2, this dependence should be reduced.

For these preliminary results, we have made an initial estimate of the model dependence based on changes of the branching fractions under variation of the form factor calculation or model. The previous analysis found that the error on the branching fraction obtained from comparison of models was larger than that obtained by variation of a particular form factor parameterization within the uncertainties ascribed by the relevant authors. Such variations will be investigated for the final result. Table IV shows the variation for $\pi\ell\nu$ as the π and vector form factors are varied. We have included in the set of models those which have the most extreme variations in shape of $d\Gamma/dq^2$. For $\pi\ell\nu$, we find our procedure results in almost no sensitivity to the form factor used for the signal mode efficiencies. A larger sensitivity is seen to variation of the vector mode form factors because of cross feed from those modes. Overall, the sensitivity is substantially reduced from that seen in the previous analysis.

To assign uncertainties, we use an empirical observation from the original analysis. For that analysis, for any given model we varied the internal parameters to determine an error on the rates extracted within that model. We then defined a range of potential branching fractions by taking the model with the lowest result and subtracting one standard deviation

TABLE IV: Branching fractions $\mathcal{B}(B^0 \to \pi^- \ell^+ \nu)$ obtained under variation of the π form factor model. Shown are the results for the total branching fraction, the partial branching fraction in each q^2 bin, the $-2\ln L$ for the fit, and the fit probability. Branching fraction uncertainties are statistical only. The bottom two rows tabulate the estimated model dependence using the method described in the text. All rates are in units 10^{-4}.

			q^2 interval (GeV^2)				
π Model	ρ Model	$\mathcal{B}_{\text{total}}$	$\mathcal{B}_{<8}$	$\mathcal{B}_{8-16}$	$\mathcal{B}_{\geq 16}$	$-2\ln L$	$P(\chi^2)$
Ball'01	Ball'98	1.38 ± 0.18	0.427 ± 0.109	0.687 ± 0.107	0.261 ± 0.095	390.5	0.41
ISGW2	Ball'98	1.38 ± 0.18	0.426 ± 0.110	0.696 ± 0.109	0.253 ± 0.091	390.8	0.41
SPD	Ball'98	1.37 ± 0.18	0.434 ± 0.109	0.686 ± 0.107	0.245 ± 0.090	389.8	0.42
Ball'01	ISGW2	1.46 ± 0.18	0.449 ± 0.109	0.722 ± 0.107	0.291 ± 0.094	391.0	0.41
ISGW2	ISGW2	1.46 ± 0.18	0.448 ± 0.110	0.732 ± 0.108	0.283 ± 0.091	391.2	0.40
SPD	ISGW2	1.45 ± 0.18	0.454 ± 0.109	0.721 ± 0.106	0.275 ± 0.089	390.2	0.42
Ball'01	Melikhov'00	1.32 ± 0.18	0.431 ± 0.109	0.671 ± 0.108	0.217 ± 0.095	390.6	0.41
Ball'01	UKQCD'98	1.41 ± 0.18	0.434 ± 0.109	0.698 ± 0.107	0.275 ± 0.094	390.1	0.42
π 1.7×RMS	Ball'98	0.008	0.006	0.008	0.011		
Ball'01	ρ 1.7×RMS	0.102	0.016	0.036	0.054		

from the variations within that model, and taking the model with the highest result, and adding one standard deviation. Our assigned uncertainty covered 70% of this range. (Note that this procedure gave us a more conservative range than taking one half the spread among models). Empirically, we found that this procedure agreed with taking 1.7 times the rms spread among models for all quantities that we examined. For these preliminary results, we therefore apply this latter procedure. The results are also summarized in Table IV.

We stress that the form factors from any given model are *not* used to constrain the relative rates extracted in each of the three q^2 regions. Only the efficiencies within each q^2 range are modified. Hence the quality of the fit used to extract the rates does not discriminate among different form factor descriptions. This discrimination is discussed in the following section.

VII. EXTRACTION OF $|V_{ub}|$ AND DISCRIMINATION OF MODELS

We extract $|V_{ub}|$ from the measured rates for $\pi\ell\nu$ only. The $\rho\ell\nu$ mode at this time has too large an uncertainty. In particular the ρ is uncomfortably sensitive to the details of the $X_u\ell\nu$ background in this analysis, and while we can characterize the size of the uncertainty, it is difficult to assign a precise, well-understood uncertainty.

For $\pi\ell\nu$, we first explore fitting q^2 distributions from various form factor predictions to the rates extracted from the three q^2 distributions. To be self-consistent, we extract $|V_{ub}|$ for a particular form factor using the rates from the fit with that model. In practice, as we have seen, this makes little difference in this analysis. Since each model predicts the total rate modulo $|V_{ub}|$, $|V_{ub}|$ becomes the one free parameter for the fit that normalizes the prediction to the observed rates. The quality of the fit measures how well the form factor shape describes the data, so provides one means of discrimination among form factors. The results of this procedure are summarized in Table V. For the three calculations that have been used for both efficiency and $|V_{ub}|$ extraction, the data rates with the best fits for each predicted form factor are shown in Figure 10. Note that the probability of χ^2 for the ISGW II

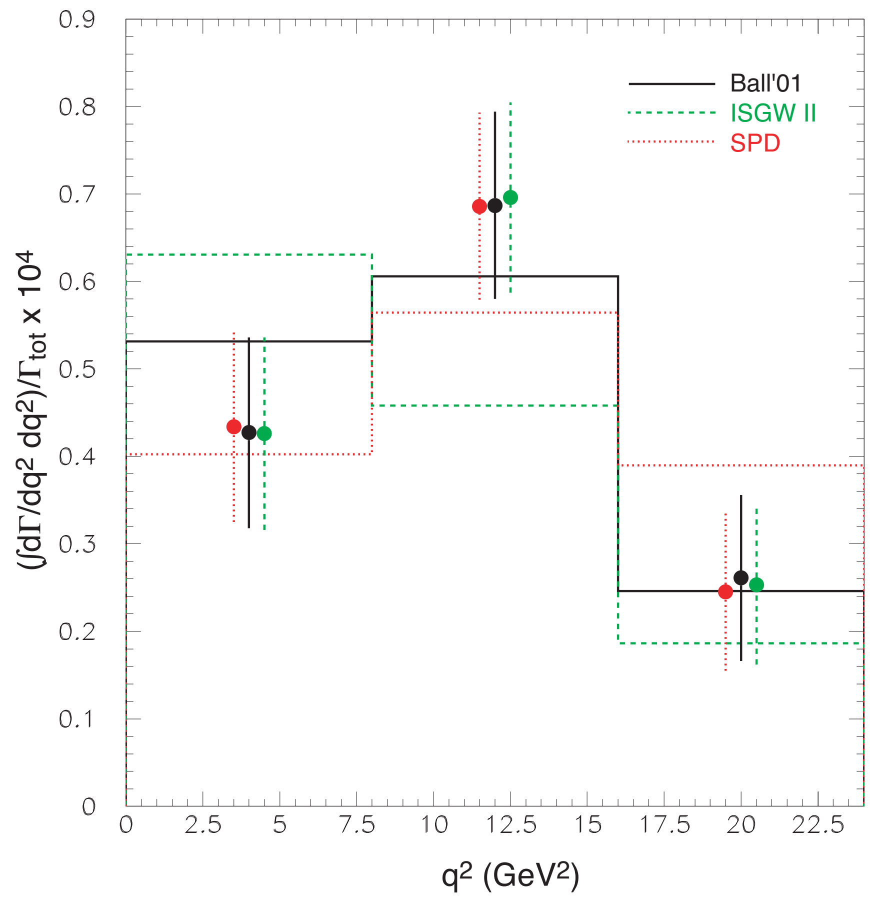

FIG. 10: Branching fractions in the restricted q^2 intervals for $B^0 \to \pi^- \ell^+ \nu$ (points) and the best fit to the predicted $d\Gamma/dq^2$ (histograms) for the three models used to extract both rates and $|V_{ub}|$. The data points have small horizontal offsets introduced for clarity. The last bin has been artificially truncated at 24 GeV^2 in the plot – the information out to $q^2_{\rm max}$ has been included in the work.

model is of order one percent or less, indicating that this model is likely to be unreliable for determination of $|V_{ub}|$ from $\pi\ell\nu$. Note further that the spread among the central values from the various calculations is fairly small relative to the uncertainties quoted in the calculations themselves.

To determine the effect of the systematic uncertainties, we repeat the above fit using three q^2 rates obtained from the branching ratio fit after each systematic variation. This procedure automatically accounts for correlations among the three intervals. We then increase the uncertainty for each variation by one half of the fractional error introduced by the second term in Equation 5.

As we discuss below, each of the form factor calculations used to extract $|V_{ub}|$ from the full q^2 range has some measure of model dependence. To allow for this additonial model dependence, we consider two methods of assigning a "theoretical" uncertainty. We first examine the minimum value $V_{\rm min}$ and the maximum value $V_{\rm max}$ when we increase or decrease the rate prediction by one theoretical standard deviation for all of the models considered. Due to the poor agreement of the ISGW II form factor with the $\pi\ell\nu$ data, we do not consider it. We then assign an asymmetric error based on 70% of the deviation relative to the nominal central value – that is, we take $0.7(V_{\rm max} - V_{\rm nom})$ and $0.7(V_{\rm nom} - V_{\rm min})$. Because the result

TABLE V: $|V_{ub}|$ extracted from fits to the rates measured in the three q^2 intervals for a variety of form factors for $\pi\ell\nu$. The table indicates form factor calculation, $|V_{ub}|$ with statistical error only, predicted $\Gamma_\pi^{\rm th}/|V_{ub}|^2$ with the estimated theoretical uncertainty, the χ^2 for the fit, and the probability of χ^2 given the two degrees of freedom.

π Model	ρ Model	$\|V_{ub}\| \times 10^3$	$\Gamma_\pi^{\rm th}/\|V_{ub}\|^2$ (ps^{-1})	Fit χ^2	$P(\chi^2)$
Ball'01	Ball'98	3.25 ± 0.21	$8.4^{+3.5}_{-2.4}$	1.5	0.47
KRWWY[a]	Ball'98	3.44 ± 0.23	7.3 ± 2.5	6.3	0.04
ISGW2	Ball'98	2.92 ± 0.20	9.6 ± 4.8	8.7	0.01
SPD	Ball'98	3.01 ± 0.19	9.6 ± 2.9	4.0	0.14
Ball'01	ISGW2	3.34 ± 0.20	$8.4^{+3.5}_{-2.4}$	1.8	0.42
ISGW2	ISGW2	3.01 ± 0.19	9.6 ± 4.8	10.1	0.007
SPD	ISGW2	3.10 ± 0.19	9.6 ± 2.9	3.8	0.15
Ball'01	Melikhov'00	3.20 ± 0.21	$8.4^{+3.5}_{-2.4}$	1.3	0.53
Ball'01	UKQCD'98	3.28 ± 0.20	$8.4^{+3.5}_{-2.4}$	1.6	0.45

[a]Uses rates determined with the Ball'01 form factor.

obtained using Ball'01 is close to the mean, we take that result as the nominal value. Note that when a symmetric theory error is quoted on the rate, we re-interpret that error as symmetric on the amplitude. To be precise, we map $\gamma_{\rm th} \pm \sigma_{\rm th}$ to $\gamma_{\rm th} \pm \sigma_{\rm th}(1 \pm \sigma_{\rm th}/(4\gamma_{\rm th})$. This procedure yields

$$|V_{ub}| = (3.25 \pm 0.21 \; {}^{+0.16}_{-0.18} \; {}^{+0.63}_{-0.44} \pm 0.12 \pm 0.07) \times 10^{-3}, \tag{6}$$

where the errors are statistical, experimental systematic and the estimated uncertainties from the $\pi\ell\nu$ form factor, the $\rho\ell\nu$ form factors, and from modeling other $B \to X_u\ell\nu$ decays. Taking one half, rather than 70%, as the scale factor, yields $|V_{ub}| = (3.25 \pm 0.21 \; {}^{+0.16}_{-0.18} \; {}^{+0.45}_{-0.32} \pm 0.12 \pm 0.07) \times 10^{-3}$ Alternatively, we add in quadrature the rms spread among the central values from different form factors to the theoretical uncertainty. Ball'01 quotes the largest uncertainty, and taking this uncertainty and the rms spread of 0.21, we obtain

$$|V_{ub}| = (3.25 \pm 0.21 \; {}^{+0.16}_{-0.18} \; {}^{+0.64}_{-0.56} \pm 0.12 \pm 0.07) \times 10^{-3}. \tag{7}$$

We take the latter as the suggested result. Note that the error on $|V_{ub}|$ from the uncertainty in the rates under variation of form factors is completely dwarfed by the error arising from uncertainty in the theoretical normalization of the form factor.

While in principle form factors determined from light cone sum rules (LCSR) and from lattice calculations are truly QCD-based calculations and not models, these calculations are valid over a restricted q^2 region. The LCSR assumptions are expected to break down for $q^2 \geq 16 GeV^2$, while the current lattice calculations are valid only for $q^2 \gtrsim 16 GeV^2$. Extrapolation beyond these ranges therefore introduces a model dependence in the form used for the extrapolation. To minimize this uncertainty, we extract $|V_{ub}|$ from these more restricted regions. The results are shown in Table VI. Note that even in the region $q^2 \geq 16 GeV^2$, model dependence can result in the lattice calculations via the interpolation procedures used to integrate over the lattice points.

Taking 70% of the full range and the FNAL central value (which is almost exactly the mean of the results), we summarize the lattice–based results as

$$|V_{ub}|_{q^2 \geq 16 {\rm GeV}^2} = (2.96 \pm 0.54 \; {}^{+0.26}_{-0.27} \; {}^{+0.98}_{-0.50} \pm 0.31 \pm 0.09) \times 10^{-3}. \tag{8}$$

TABLE VI: Values for $|V_{ub}|$ obtained using form factors (FF) from light cone sum rules in the q^2 interval $0-16$ GeV^2 (top two rows) and from lattice QCD for $q^2 \geq 16$ GeV^2 (bottom five rows). Only the statistical errors are indicated. The data rates obtained using Ball'01 for $\pi\ell\nu$ and Ball'98 for $\rho\ell\nu$ were used as the input for all values obtained.

π FF	$\lvert V_{ub}\rvert \times 10^3$	$\Gamma_\pi^{\rm th}/\lvert V_{ub}\rvert^2$ (ps^{-1})	Fit χ^2	$P(\chi^2)$
Ball'01	3.24 ± 0.22	$6.9^{+2.4}_{-1.8}$	1.5	0.22
KRWWY	3.45 ± 0.25	5.7 ± 1.9	6.1	0.013
FNAL[a]	2.96 ± 0.54	$1.91^{+0.55}_{-0.33}$	–	–
JLQCD[b]	3.13 ± 0.57	1.71 ± 0.76	–	–
APE method 1[c]	3.34 ± 0.61	1.5 ± 0.7	–	–
APE method 2[c]	2.82 ± 0.51	2.1 ± 1.1	–	–
UKQCD[c]	2.70 ± 0.49	$2.3^{+0.92}_{-0.72}$	–	–

[a]The authors of [15] have provided the rate integrated over this range and the corresponding uncertainty.

[b]The authors of [16] have provided the rate integrated over this range and the corresponding uncertainty.

[c]We have integrated the rate using their FF parameterization over the restricted q^2 interval and scaled their uncertainties accordingly.

In this case the RMS spread in the central values is 0.25×10^{-3}. Taking the simple average of the two LCSR values and again using the 70% range, we characterize the LCSR results as

$$|V_{ub}|_{q^2<16\mathrm{GeV}^2} = (3.35 \pm 0.23 \;^{+0.17}_{-0.19} \;^{+0.55}_{-0.39} \pm 0.12 \pm 0.07) \times 10^{-3}. \tag{9}$$

We average the lattice and LCSR results, with a preliminary attempt to consider the correlated experimental systematics. We also treat the theoretical systematics as largely correlated, and we obtain

$$|V_{ub}| = (3.32 \pm 0.21 \;^{+0.17}_{-0.19} \;^{+0.55}_{-0.39} \pm 0.12 \pm 0.07) \times 10^{-3}, \tag{10}$$

which has somewhat smaller theoretical uncertainties.

The variations in $|V_{ub}|$ and our averages our illustrated in Figure 11.

VIII. SUMMARY

With a sample of 9.7×10^6 $B\bar{B}$ pairs, CLEO has studied B decays to $\pi\ell\nu$, $\rho\ell\nu$, $\omega\ell\nu$, and $\eta\ell\nu$ where $\ell = e$ or μ. From the combination of a broad momentum range for the charged lepton momentum and from independent extraction of rates in three separate q^2 intervals, we were able to reduce the uncertainties from modelling within the form factors calculations. For the decay $B^0 \to \pi^-\ell^+\nu$, we have determined the branching fractions

$$\begin{aligned} \mathcal{B}(0 \leq q^2 < 8\,\mathrm{GeV}^2) &= (0.427 \pm 0.109 \;^{+0.046}_{-0.051} \pm 0.006 \pm 0.016 \pm 0.001) \times 10^{-4} \\ \mathcal{B}(8 \leq q^2 < 16\,\mathrm{GeV}^2) &= (0.687 \pm 0.107 \;^{+0.082}_{-0.089} \pm 0.008 \pm 0.036 \pm 0.008) \times 10^{-4} \\ \mathcal{B}(q^2 \geq 16\,\mathrm{GeV}^2) &= (0.261 \pm 0.095 \;^{+0.046}_{-0.048} \pm 0.011 \pm 0.054 \pm 0.015) \times 10^{-4}. \end{aligned} \tag{11}$$

Combining these rates and taking into account correlated systematics uncertainties, we obtain

$$\mathcal{B}(B^0 \to \pi^-\ell^+\nu) = (1.376 \pm 0.180 \;^{+0.116}_{-0.135} \pm 0.008 \pm 0.102 \pm 0.021) \times 10^{-4}, \tag{12}$$

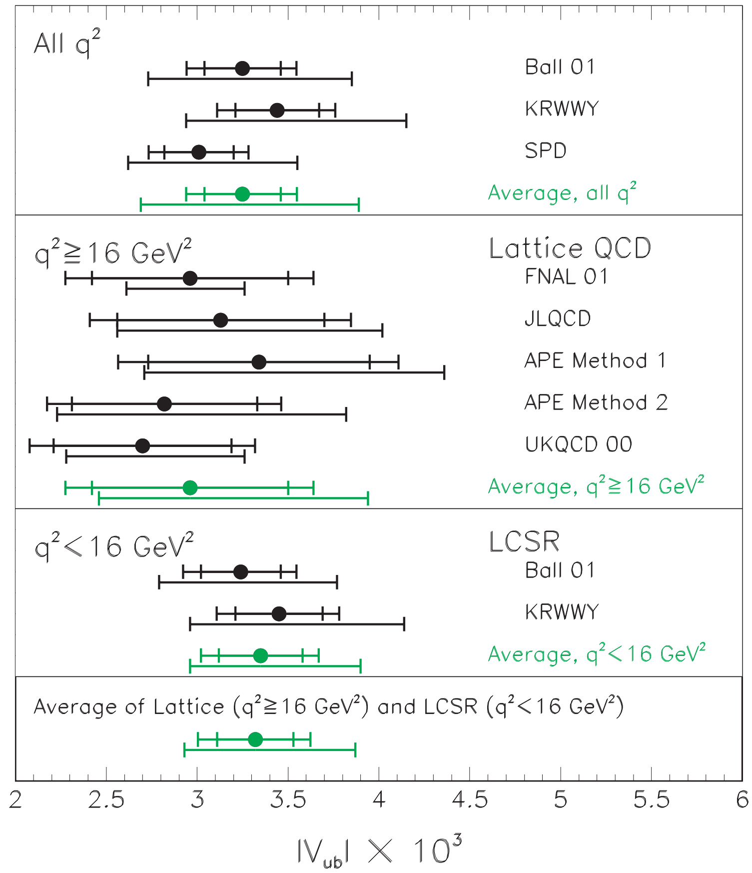

FIG. 11: Values for $|V_{ub}|$ obtained using the entire q^2 range for the various form factor calculations (top block), using lattice QCD for $q^2 \geq 16$ GeV^2 (second block), using LCSR for $q^2 < 16$ GeV^2 (third block), and our average of the last two (bottom block). In all cases, the top bar indicates the statistical and all the experimental systematics (combined in quadrature), the lower bar indicated the range of motion due to the theoretical uncertainties. The green "average" indicates our determination of a representative value in each category.

where the errors are statistical, experimental systematic and the estimated uncertainties from the $\pi\ell\nu$ form factor, the $\rho\ell\nu$ form factors, and from modeling other $B \to X_u\ell\nu$ decays. At the stage of this preliminary result, the uncertainties in $\rho\ell\nu$ from modelling of the $B \to X_u\ell\nu$ feeddown are large. We have included the rates obtained for completeness, but consider this result too preliminary for use in averages and, in particular, for use in the extraction of $|V_{ub}|$.

We see evidence for the decay $B^{\pm} \to \eta\ell^{\pm}\nu$ with a statistical significance corresponding roughly to 3.4σ. The rate we obtain,

$$\mathcal{B}(B^+ \to \eta\ell^+\nu) = (0.85 \pm 0.31 \pm 0.14) \times 10^{-4}, \tag{13}$$

is consistent, within sizable errors, with that expected from the measured pion rate and isospin relations. Only an ISGW II form factor has been examined, and no model dependence has been assigned at this time.

From the $\pi\ell\nu$ q^2 behavior that we have obtained, we find the ISGW II form factor for $\pi\ell\nu$ consistent with data at only the 1% level. We therefore exclude this model from the extraction of $|V_{ub}|$ using this mode.

By fitting various form factor calculations to the observed q^2 behavior, we extract

$$|V_{ub}| = (3.25 \pm 0.21 \ {}^{+0.16}_{-0.18} \ {}^{+0.64}_{-0.56} \pm 0.12 \pm 0.07) \times 10^{-3}, \tag{14}$$

where the errors are statistical, experimental systematic and the estimated uncertainties from the $\pi\ell\nu$ form factor, the $\rho\ell\nu$ form factors, and from modeling other $B \to X_u\ell\nu$ decays.

In a preliminary attempt to reduce modelling uncertainties, we extract $|V_{ub}|$ using a $\pi\ell\nu$ form factor from light cone sum rules in the range $q^2 < 16$ GeV^2 and from lattice QCD above this range. An average of these results, with a preliminary attempt to take correlated systematics into account and with a conservative assumption that the theoretical uncertainties are largely correlated, we obtain

$$|V_{ub}| = (3.32 \pm 0.21 \ {}^{+0.17}_{-0.19} \ {}^{+0.55}_{-0.39} \pm 0.12 \pm 0.07) \times 10^{-3}. \tag{15}$$

The model dependence is somewhat reduced.

These results supersede the $\pi\ell\nu$ results obtained in reference [3]. We have not yet combined these results with those from reference [4], for which many of the systematics will be correlated.

All results are preliminary.

In closing, we note that there is an *ad hoc* element in any uncertainty ascribed to the form factor dependence of these results. The definition is therefore likely to vary from experiment to experiment. Anyone comparing the experimental results must therefore ensure a uniform method is applied in the comparison.

We thank A. Kronfeld, J. Simone, T. Onogi, T. Feldmann, P. Kroll, C. Maynard and D. Melikhov. for assistance with form factors. We gratefully acknowledge the effort of the CESR staff in providing us with excellent luminosity and running conditions. M. Selen thanks the PFF program of the NSF and the Research Corporation, and A.H. Mahmood thanks the Texas Advanced Research Program. This work was supported by the National Science Foundation, and the U.S. Department of Energy and the Natural Sciences and Engineering Research Council of Canada.

---

[1] N. Cabibbo, Phys. Rev. Lett. **10**, 531, (1963). M. Kobayashi and T. Maskawa, Prog. Theor. Phys. **49**, 652 (1973).

[2] M. Battaglia and L. Gibbons, *Determination of* $|V_{ub}|$, in *Review of Particle Properties*, K. Hagiwara et al., Phys. Rev. D 66 010001 (2002).

[3] J. Alexander *et al.* (CLEO Collaboration), Phys. Rev. Lett. **77**, 5000 (1996).

[4] B.H. Behrens *et al.* (CLEO Collaboration), Phys. Rev. **D61**, 052001 (2000).

[5] A. Abada *et al.*, Nucl. Phys. B **416** (1994) 675 [arXiv:hep-lat/9308007]

[6] C. R. Allton *et al.* [APE Collab.], Phys. Lett. B **345**, 513 (1995) [arXiv:hep-lat/9411011]

[7] L. Del Debbio, J. M. Flynn, L. Lellouch and J. Nieves [UKQCD Collab.], Phys. Lett. B **416**, 392 (1998) [arXiv:hep-lat/9708008]

[8] S. Hashimoto, K. I. Ishikawa, H. Matsufuru, T. Onogi and N. Yamada, Phys. Rev. D **58**, 014502 (1998) [arXiv:hep-lat/9711031]

[9] S. Ryan, A. El-Khadra, S. Hashimoto, A. Kronfeld, P. Mackenzie and J. Simone, Nucl. Phys. Proc. Suppl. **73**, 390 (1999) [arXiv:hep-lat/9810041]

[10] S. M. Ryan, A. X. El-Khadra, A. S. Kronfeld, P. B. Mackenzie and J. N. Simone, Nucl. Phys. Proc. Suppl. **83**, 328 (2000) [arXiv:hep-lat/9910010]
[11] L. Lellouch, [arXiv:hep-ph/9912353]
[12] K. C. Bowler *et al.* [UKQCD Collab.], Phys. Lett. B **486**, 111 (2000) [arXiv:hep-lat/9911011]
[13] D. Becirevic and A. B. Kaidalov, Phys. Lett. B **478**, 417 (2000) [arXiv:hep-ph/9904490]
[14] S. Aoki *et al.* [JLQCD Collab.], Nucl. Phys. Proc. Suppl. **94**, 329 (2001) [arXiv:hep-lat/0011008]
[15] A. X. El-Khadra, A. S. Kronfeld, P. B. Mackenzie, S. M. Ryan and J. N. Simone, Phys. Rev. D **64**, 014502 (2001) [arXiv:hep-ph/0101023]
[16] S. Aoki *et al.* [JLQCD Collab.], Phys. Rev. D **64**, 114505 (2001) [arXiv:hep-lat/0106024]
[17] A. Abada, D. Becirevic, P. Boucaud, J. P. Leroy, V. Lubicz and F. Mescia, Nucl. Phys. B **619**, 565 (2001) [arXiv:hep-lat/0011065]
[18] P. Ball and V. M. Braun, Phys. Rev. D **55**, 5561 (1997) [arXiv:hep-ph/9701238]
[19] P. Ball and V. M. Braun, Phys. Rev. D **58**, 094016 (1998) [arXiv:hep-ph/9805422]
[20] A. Khodjamirian, R. Rückl, S. Weinzierl and O. I. Yakovlev, Phys. Lett. B **410**, 275 (1997) [arXiv:hep-ph/9706303]
[21] A. Khodjamirian, R. Rückl, S. Weinzierl, C. W. Winhart and O. I. Yakovlev, Phys. Rev. D **62**, 114002 (2000) [arXiv:hep-ph/0001297]
[22] A. P. Bakulev, S. V. Mikhailov and R. Ruskov, [arXiv:hep-ph/0006216]
[23] T. Huang, Z. Li and X. Wu, [arXiv:hep-ph/0011161]
[24] W. Y. Wang and Y. L. Wu, Phys. Lett. B **515**, 57 (2001) [arXiv:hep-ph/0105154]
[25] W. Y. Wang and Y. L. Wu, Phys. Lett. B **519**, 219 (2001) [arXiv:hep-ph/0106208]
[26] P. Ball and R. Zwicky, JHEP **0110**, 019 (2001) [arXiv:hep-ph/0110115]
[27] M. Wirbel, B. Stech and M. Bauer, Z. Phys. C **29**, 637 (1985)
[28] J. G. Korner and G. A. Schuler, Z. Phys. C **38**, 511 (1988) [Erratum-ibid. C **41**, 690 (1988)]
[29] N. Isgur, D. Scora, B. Grinstein and M. B. Wise, Phys. Rev. D **39**, 799 (1989)
[30] D. Scora and N. Isgur, Phys. Rev. D **52**, 2783 (1995) [arXiv:hep-ph/9503486]
[31] D. Melikhov, Phys. Rev. D **53**, 2460 (1996) [arXiv:hep-ph/9509268]
[32] M. Beyer and D. Melikhov, Phys. Lett. B **436**, 344 (1998) [arXiv:hep-ph/9807223]
[33] R. N. Faustov, V. O. Galkin and A. Y. Mishurov, Phys. Rev. D **53**, 6302 (1996) [arXiv:hep-ph/9508262]
[34] N. B. Demchuk, P. Y. Kulikov, I. M. Narodetsky and P. J. O'Donnell, Phys. Atom. Nucl. **60**, 1292 (1997) [Yad. Fiz. **60N8**, 1429 (1997)] [arXiv:hep-ph/9701388]
[35] I. L. Grach, I. M. Narodetsky and S. Simula, Phys. Lett. B **385**, 317 (1996) [arXiv:hep-ph/9605349]
[36] Riazuddin, T. A. Al-Aithan and A. H. Gilani, [arXiv:hep-ph/0007164]
[37] D. Melikhov and B. Stech, Phys. Rev. D **62**, 014006 (2000) [arXiv:hep-ph/0001113]
[38] T. Feldmann and P. Kroll, Eur. Phys. J. C **12**, 99 (2000) [arXiv:hep-ph/9905343]
[39] J. M. Flynn and J. Nieves, Phys. Lett. B **505**, 82 (2001) [arXiv:hep-ph/0007263]
[40] M. Beneke and T. Feldmann, Nucl. Phys. B **592**, 3 (2001) [arXiv:hep-ph/0008255]
[41] H. M. Choi and C. R. Ji, Phys. Lett. B **460**, 461 (1999) [arXiv:hep-ph/9903496]
[42] T. Kurimoto, H. n. Li and A. I. Sanda, Phys. Rev. D **65**, 014007 (2002) [arXiv:hep-ph/0105003]
[43] Z. Ligeti and M. B. Wise, Phys. Rev. D **53**, 4937 (1996) [arXiv:hep-ph/9512225]
[44] E. M. Aitala *et al.* [E791 Collab.], Phys. Rev. Lett. **80**, 1393 (1998) [arXiv:hep-ph/9710216]
[45] G. Burdman and J. Kambor, Phys. Rev. D **55**, 2817 (1997) [arXiv:hep-ph/9602353]
[46] L. Lellouch, Nucl. Phys. B **479**, 353 (1996) [arXiv:hep-ph/9509358]

[47] T. Mannel and B. Postler, Nucl. Phys. B **535**, 372 (1998) [arXiv:hep-ph/9805425]
[48] Y. Kubota *et al.*, Nucl. Instrum. Methods Phys. Res., Sect. A **320**, 66 (1992).
[49] T.S. Hill *et al.*, Nucl. Instrum. Methods Phys. Res., Sect. A **418**, 32 (1998).
[50] Spurious CsI showers from hadronic interactions add linearly to $E_{\rm miss}$, but tend to average out in the vector sum for $\vec{P}_{\rm miss}$. Incorrect mass assignment also smears $E_{\rm miss}$.
[51] G.C. Fox and S. Wolfram, Phys. Rev. Lett. **41**, 1581 (1978).
[52] R. Brun *et al.*, GEANT 3.15, CERN DD/EE/84-1.
[53] F. De Fazio and M. Neubert, JHEP **9906**, 017 (1999).
[54] A.L. Kagan and M. Neubert, Eur. Phys. J. **C7**, 5 (1999).
[55] S. Chen *et al.* (CLEO Collaboration), Phys. Rev. Lett. **87**, 251807 (2001).
[56] A. Bornheim *et al.* (CLEO Collaboration), Phys. Rev. Lett. **88**, 231803 (2002).
[57] D.E. Groom *et al.* (Particle Data Group), Eur. Phys. J. **C15**, 1 (2000).
[58] R. Barlow and C. Beeston, Comput. Phys. Commun., **77**, 219 (1993).